RBMX2: A Pivotal Regulator Linking *Mycobacterium bovis* Infection to Epithelial-Mesenchymal Transition and Lung Cancer Progression

Chao Wang[1,2,8] Yongchong Peng[1,2] Hongxin Yang[3,4] Yanzhu Jiang[1,2] Abdul Karim Khalid[1] Kailun Zhang[1,2] Shengsong Xie[1] Luiz Bermudez[5] Yong Yang[6] Lei Zhang[1,2] Huanchun Chen[1] Aizhen Guo[1,2,7]* Yingyu Chen[1,2*]

1 The National Key Laboratory of Agricultural Microbiology, College of Veterinary Medicine, Huazhong Agricultural University, Wuhan, China, 430000

2 National Animal Tuberculosis Para-Reference Laboratory (Wuhan) of Ministry of Agriculture and Rural Affairs, Huazhong Agricultural University, Wuhan, China, 430000

3 Oncology Collaborative Innovation Center, Inner Mongolia Medical University, Hohhot, Inner Mongolia, China, 01000

4 Oncology Collaborative Innovation Center, Inner Mongolia Medical University, Hohhot, Inner Mongolia, China, 010000

5 Department of Biomedical Sciences, College of Veterinary Medicine, Oregon State University, Corvallis, OR, United States, 97331

6 Department of Surgical Oncology, People's Hospital of Inner Mongolia Autonomous Region, Hohhot, Inner Mongolia, China, 010000

7 Hubei Hongshan Laboratory, Huazhong Agricultural University, Wuhan, China, 430000

8 Center for Infectious Disease Research, School of Medicine, Westlake University, Hangzhou, Zhejiang, China, 310012

.

Correspondence*: Yingyu Chen, chenyingyu@mail.hzau.edu.cn, +86 15972025761

Aizhen Guo, aizhen@mail.hzau.edu.cn.+86 13100712906

Abstract

The emergence and progression of tuberculosis (TB) result from the intricate interplay among the pathogen, host, and environmental factors. In 2022, there were 10.6 million new TB cases reported globally, leading to 1.3 million deaths. In regions with a high prevalence of zoonotic TB, *Mycobacterium bovis* (*M. bovis*) accounts for approximately 10% of human TB cases. The immune evasion mechanisms and latent infections of *Mycobacterium tuberculosis* (*M. tb*) complicate our understanding of the host immune response to TB. This study identifies a novel host factor, RNA-binding motif protein X-linked 2 (RBMX2), which shows potential against *M. bovis* infection. However, the specific molecular mechanisms and roles of RBMX2 during *M. bovis* infection remain poorly understood. Our investigations revealed that following infection, RBMX2 was highly expressed in various cell types, including embryonic bovine lung (EBL) cells, bovine macrophage (BoMac) cells, bovine lung alveolar primary cells, and human pulmonary alveolar epithelial cells (A549). Using a multifaceted approach that included global transcriptional sequencing, proteomics, cell adhesion assays, ChIP-PCR, and Western blot analyses, we demonstrated that RBMX2 inhibits cell adhesion and tight junction formation in EBL cells while promoting the adhesion and invasion of *M. bovis* through the activation of the p65 pathway. Furthermore, our data suggest that RBMX2 regulates epithelial-mesenchymal transition (EMT), a process strongly associated with cancer, as indicated by our global transcriptomics, proteomics, and metabolomics analyses. To further explore the relationship between RBMX2 and cancer, we analyzed the TIMER2.0 database and found elevated expression levels of RBMX2 in lung adenocarcinoma (LUAD) and lung squamous carcinoma (LUSC) tissues compared to normal lung tissues. This finding was corroborated by immunofluorescence validation. After constructing an *M. bovis*-infected BoMac-induced EBL-EMT model, we confirmed that RBMX2 contributes to EMT by activating the p65/MMP-9 pathway post-infection.

This study elucidates the role of *RBMX2* as a novel host factor with potential anti-TB functions that inhibit TB-induced EMT. These insights have vital implications for the development of TB vaccines and therapeutic strategies for TB-mediated lung cancer, highlighting *RBMX2* as a promising target for future research.

Keywords: *Mycobacterium bovis*, RNA-binding motif protein X-linked 2, embryo bovine lung, bovine macrophage, cell tight junction, epithelial–mesenchymal transition, bovine tuberculosis, cell tight junction

Abbreviations

RBMX2 RNA-binding motif protein X-linked 2; EBL embryo bovine lung cells; BoMac bovine macrophage cells; A549 human pulmonary alveolar epithelial cells; TB tuberculosis; *M. bovis Mycobacterium bovis*; *M. tb Mycobacterium tuberculosis*; BCG *Bacillus* Calmette–Guerin; WOAH World Organisation for Animal Health; hpi hours postinfection; *M. smegmatis Mycobacterium smegmatis*; *E. coli Escherichia coli*; p65 RELA proto-oncogene, NF-kB subunit;MAPK mitogen-activated protein kinase; EMT epithelial–mesenchymal transition; PARP poly ADP-ribose polymerase; ZO-1 tight junction protein 1; CLDN-5 claudin 5; OCLN occludin; MMP-9 matrix metallopeptidase 9; SP-A surfactant protein A; GO Gene Ontology; KEGG Kyoto Encyclopedia of Genes and Genomes; WB Western blot; RT-qPCR real-time quantitative polymerase chain reaction; IF immunofluorescence; ECM extracellular matrix; TCGA the cancer genome atlas

Introduction

Tuberculosis (TB) remains a significant global health challenge, with approximately 10.6 million new cases reported in 2022, leading to 1.3 million deaths worldwide [1]. *Mycobacterium tuberculosis* (*M. tb*) variant *Mycobacterium bovis* (*M. bovis*), a zoonotic pathogen, accounts for approximately 10% of human TB cases in regions with high prevalence of zoonotic diseases. The immune evasion mechanisms employed by *M. tb* pose challenges in understanding the host immune response and the progression of TB.

Recent studies have highlighted the interplay between chronic infections, such as TB, and cancer development [2, 3]. Emerging evidence suggests that the inflammatory environment induced by persistent infections can contribute to cellular transformations associated with epithelial-mesenchymal transition (EMT), a process linked to cancer metastasis [4]. However, the specific mechanisms underlying this relationship, particularly concerning host factors involved in TB infection, remain poorly understood.

88 In this context, we focus on RNA-binding motif protein X-linked 2 (RBMX2), a host factor that
89 has emerged as a potential modulator of both TB infection and cancer progression. In previous
90 studies, we also reported that RBMX2 can regulate the retention of APAF-1 introns through
91 alternative splicing, mediating apoptosis following *M. bovis* infection [5]. Moreover, previous research
92 also indicates that RBMX displays significant and contrasting effects depending on the tumor type,
93 functioning either as an oncogene or a tumor suppressor. For instance, its overexpression has
94 been associated with hepatocellular carcinoma [6] and T-cell lymphomas[7], while a reduction in
95 RBMX levels has been noted in Pancreatic ductal adenocarcinoma[8], suggesting a role in
96 tumorigenesis and metastasis. However, RBMX2 involvement in TB infection and its regulatory
97 effects on EMT have not been thoroughly investigated.
98 This study aims to elucidate the role of RBMX2 in *M. bovis* infection and its impact on EMT
99 in epithelial cells. We hypothesize that RBMX2 promotes the adhesion and invasion of *M. bovis* in
100 host cells while facilitating the EMT process through the activation of the p65/MMP-9 signaling
101 pathway. By investigating these interactions, we seek to provide insights into the potential dual
102 role of RBMX2 in TB and lung cancer, highlighting its significance as a therapeutic target.
103
104 **Results**
105 **Elevated expression of RBMX2 in *Mycobacterium bovis*-infected cells and tuberculous**
106 **Lesions**
107 *M. bovis* was used to infect the EBL cell library that was constructed using CRISPR/Cas9
108 technology in our laboratory at a multiplicity of infection (MOI) of 100:1. We assessed cell
109 survival and conducted high-throughput sequencing on the viable cells to identify key host
110 factors with potential anti-*M. bovis* capabilities. Notably, the RBMX2 knockout cells exhibited
111 significant resistance to the infection.
112 Further analysis using AlphaFold multimer revealed that amino acid positions 56–134 of
113 *RBMX2* contain an RNA recognition sequence (Supplementary Fig. 1A). Additionally, we identified
114 611 RBM family sequences at the bovine protein exon level and categorized them into
115 subfamilies based on motif similarity. *RBMX2* was primarily classified within subfamily VII, which
116 includes proteins such as *EIF3G*, *RBM14*, *RBM42*, *RBMX44*, *RBM17*, *PUF60*, *SART3*, and *RBM25*

117 (Supplementary Fig. 1B). A comparison of amino acid sequences indicated a high degree of
118 conservation of RBMX2 across different species (Supplementary Table 1).

119 To further confirm *RBMX2* expression in EBL cells following infection with *M. bovis* and *M.*
120 *bovis* Bacillus Calmette–Guerin (BCG), we collected RNA samples at 24, 48, and 72 hours
121 post-infection (hpi). Real-time quantitative polymerase chain reaction (RT-qPCR) results
122 demonstrated that *RBMX2* expression was significantly upregulated after both *M. bovis* and *M.*
123 *bovis* BCG infections (Figs. 1A and B). Moreover, elevated *RBMX2* levels were observed in bovine
124 lung macrophages (BoMac cells), bovine lung alveolar primary cells, and human lung epithelial
125 cells (A549 cells) following *M. bovis* infection (Figs. 1C-E).

126 Additionally, we investigated *RBMX2* expression in clinical tissue samples from cows affected
127 by *M. bovis*. Livers and lung samples with visible tuberculous lesions were obtained from a
128 slaughterhouse. RT-qPCR analysis revealed that *RBMX2* expression was upregulated in both the
129 lungs and livers infected with *M. bovis* (Fig. 1F).

130

131

132 ***RBMX2* did not affect cell proliferation but inhibited epithelial cell survival during *M. bovis***
133 **infection**

134 In generating *RBMX2* monoclonal knockout (KO) cells, monoclonal cells were selected
135 through limited dilution in 96-well plates. Sanger sequencing was conducted to identify different
136 monoclonal cells with distinct knockout sites (Supplementary Fig. 2A).

137 The impact of *RBMX2* knockout on EBL cells indicated that *RBMX2* did not alter cell
138 morphology, as evidenced by cytoskeleton staining using phalloidine (Supplementary Fig. 2B).
139 Additionally, cellular proliferation was assessed using the EDU assay (Figs. 1G and H) and CCK-8
140 assay (Fig. 1I), along with cell cycle progression evaluated by Flow cytometry (Supplementary Fig.
141 2C).

142 To investigate the potential role of *RBMX2* in resistance to *M. bovis* infection, we assessed
143 the survival rate of EBL cells and H1299 cells at different hours post-infection using CCK-8 assay.
144 The findings revealed an enhanced survival rate in both *RBMX2* knockout polyclonal and
145 monoclonal EBL cells following *M. bovis* infection (Figs. 1J and K). Furthermore, RBMX2-silenced

146 H1299 cells exhibited a higher survival rate compared to H1299 ShNc cells after *M. bovis* infection
147 (Fig. 1L). Notably, *RBMX2* knockout in EBL cells and silencing in H1299 cells demonstrated
148 significant improvements in cells survival at 96 and 120 hpi compared to Wild Type (WT) EBL cells
149 and H1299 ShNC cells, as evidenced by crystal violet staining (Supplementary Fig. 2D).
150
151 ***RBMX2*-regulated genes associated with cell tight junction and EMT-related pathways**
152 In investigate the role of *RBMX2* knockout in the process of *M. bovis* infection, we selected
153 *RBMX2* knockout EBL cells and WT EBL cells at 0 (2 hpi, recorded as 0 hpi), 24, and 48 hpi for
154 RNA-Seq analysis. A total of 16,079 genes were detected, with a significance level of $p < 0.05$ and
155 log2 (fold change) > 2 compared to WT EBL cells. Notably, 42 genes are significantly regulated at
156 all three-time points (0, 24, and 48 hpi) (Fig. 2A). Among these, 11 genes were significantly
157 upregulated, while 31 genes were significantly downregulated. A heat map illustrates the
158 expression level of each gene across various samples, with each row representing a specific gene
159 and each column representing the expression levels in a given sample (Fig. 2A).
160 The functional significance of these differentially expressed genes (DEGs) in EBL cells
161 infected with *RBMX2* knockout was further explored using GO and KEGG analyses. The most
162 significantly affected biological processes included epithelial cell differentiation, cell adhesion and
163 biological adhesion. The cellular components most affected were the extracellular region,
164 extracellular region part, extracellular space, and plasma membrane part. The molecular
165 functions primarily associated with activin receptor activity, type I (Fig. 2B).
166 The KEGG pathway entries revealed that these genes were linked to a various pathways,
167 including ECM–receptor interaction, cGMP-PKG signaling pathway, PI3K-Akt signaling pathway,
168 cytokine-cytokine receptor interaction, and vascular smooth muscle contraction (Fig. 2C).
169 Proteomics also validated these phenotypes related to cell tight junction and EMT using 48hpi
170 protein samples, highlighting pathways such as extracellular space, integrin binding, basement
171 membrane, and glucose homeostasis via GO analysis, along with cell adhesion molecules,
172 ECM-receptor interaction, and TGF-beta signaling pathway through KEGG analysis (Figs. 2D and
173 E).
174 We also examined the impact of varying infection durations on *RBMX2* knockout EBL cellular

175 lines via GO analysis. At 0 hpi, genes were primarily related to the pathways of cell junctions,
176 extracellular regions, and cell junction organization (Supplementary Fig. 3A). At 24 hpi, genes
177 were mainly associated with pathways of the basement membrane, cell adhesion, integrin
178 binding and cell migration (Supplementary Fig. 3B). By 48 hpi, genes were annotated into
179 epithelial cell differentiation and were negatively regulated during epithelial cell proliferation
180 (Supplementary Fig. 3C). This indicated that *RBMX2* can regulate cellular connectivity throughout
181 the stages of *M. bovis* infection.

182 For KEGG analysis, genes linked to the *MAPK* signaling pathway, chemical carcinogen-DNA
183 adducts, and chemical carcinogen–receptor activation were observed at 0 hpi (Supplementary Fig.
184 3D). At 24 hpi, significant enrichment was found in the ECM–receptor interaction, PI3K–Akt
185 signaling pathway, and focal adhesion (Supplementary Fig. 3E). Upon enrichment analysis at 48
186 hpi, significant enrichment was noted in the TGF-beta signaling pathway, transcriptional
187 misregulation in cancer, microRNAs in cancer, small cell lung cancer, and p53 signaling pathway
188 (Supplementary Fig. 3F).

189 To validate the RNA-seq data, we confirmed a random selection of 10 genes using RT-qPCR
190 (Fig. 2F). The mRNA levels of the selected genes were consistent with the RNA-seq outcomes,
191 including *FRMD4B*, *MCTP1*, *HSPB8*, *ST14*, and *OMD*, which are linked to scaffold proteins, cell
192 adhesion, and epithelial barriers. Additionally, *MCTP1*, *HSPB8*, *IL-24*, *1L-7*, *GPX2*, and *NOS3* were
193 associated with apoptosis, inflammation, and oxidative stress.

194

195 ***RBMX2* interferes with the integrity of tight junctions in epithelial cells caused by *M. bovis***

196 Through transcriptome sequencing, we identified 41 genes that underwent transcript
197 changes following *M. bovis* infection. Of these, 22 genes were upregulated, while 19 genes were
198 downregulated (Supplementary Figs. 4A and B). The downregulated genes were primarily
199 associated with tight junction and leukocyte transendothelial migration (Fig. 3A). In contrast, the
200 upregulated genes were mainly linked to immunity-related pathways, including the defense
201 response to viruses and regulation of viral processes (Fig. 3B).

202 Based on these finding,we hypothesized that *RBMX2* could damage the integrity of
203 epithelial cell tight junction. To validate this prediction, we constructed a model of *M.*

204 *bovis*-destroyed tight junctions in EBL cells. EBL cells were infected with *M. bovis* and we
205 subsequently performed RT-qPCR and Western blot (WB) analyses to assess the expression of cell
206 tight junction-related mRNAs (*TJP1*, *OCLN*, *CLDN-5*, and *CLDN-7*) and proteins (ZO-1, OCLN, and
207 CLDN-5). We found that the expression levels of all mRNAs and proteins was significantly reduced
208 following *M. bovis* infection compared to the uninfected coutrol (Figs. 3C and D).

209 Tight junctions are critical intercellular adhesion structures that define the permeability of
210 barrier-forming epithelial cells [9]. The ability of epithelial cells to maintain functional intercellular
211 adhesion is essential for forming a tight epithelial protective barrier [10]. To further investigate the
212 effect of *M. bovis* on epithelial cell adhesion, we conducted a cell adhesion assay, revealing a
213 significant decrease in the intercellular adhesion ratio (Fig. 3E). These results validated that *M.*
214 *bovis* can compromise the tight junction of EBL cells.

215 To explore the impact of *RBMX2* on the epithelial cells barrier, we infected RBMX2 knockout
216 and WT EBL cells with *M. bovis* and assessed the expression of epithelial barrier-related mRNAs
217 (*TJP1*, *OCLN*, and *CLDN-5*) and proteins (ZO-1, OCLN, and CLDN-5) using RT-qPCR and WB. The
218 *RBMX2* knockout EBL cells exhibited a significant upregulation of all three proteins compared to
219 WT EBL cells (Figs. 3F and G). The cell adhesion assay also demonstrated that *RBMX2* knockout
220 EBL cells displayed a heightened adhesion ratio relative to WT EBL cells (Fig. 3H).

221 Tight junctions are essential component of the epithelial barrier and can be compromised by
222 bacteria infections, contributing to inflammation [11, 12]. To investigate whether *RBMX2* mediates
223 intracellular inflammation by regulating the tightness of the epithelial barrier, we measured the
224 mRNA levels of inflammatory factors (IL-1β, TNF, and IL-6) in *RBMX2* knockout EBL cells
225 post-infection. The results showed a decrease in the expression of these inflammatory factors in
226 RBMX2 knockout EBL cells compared to WT EBL cells after *M. bovis* infection (Fig. 3I).

227 In summary, our findings indicate that *RBMX2* affects the integrity of epithelial cell tight
228 junctions, and knocking out *RBMX2* enhances tight junction formation while decreasing the
229 inflammatory response induced by *M. bovis*.

230

231 ***RBMX2* disrupted the epithelial barrier via activating *p65***

232 The MAPK pathway and NF-kappaB pathway play crucial roles in regulating tight junctions

233 between epithelial cells [13-16]. To further elucidate the regulatory mechanism of *RBMX2* in the
234 epithelial barrier's tight junctions, we found that the MAPK pathway was enriched in our
235 transcriptome sequencing data, and the potential regulatory transcription factor p65 was
236 predicted through the JASPAR database (Supplementary Table 2).

237 We assessed the phosphorylation levels of MAPK pathway proteins and p65 protein in
238 RBMX2 knockout EBL cells, revealing that the phosphorylation of p65 and MAPK/p38/JNK was
239 significantly reduced in these cells after *M. bovis* infection compared to WT EBL cells (Figs. 4A and
240 B).

241 To determine whether RBMX2 specifically regulates the MAPK/p38/JNK proteins and p65 to
242 promote tight junction disruption and decrease intercellular adhesion, *RBMX2* knockout EBL cells
243 were treated with *PMA* (*p65* activator), *Anisomycin* (*JNK* activator), and *ML141* (*p38* activator) for
244 12 h prior to *M. bovis* infection. The optimal concentrations for these activators were determined
245 through WB and CCK-8 cell viability assays, yielding 100 nm for PMA, 10 µm for *Anisomysin*, and
246 10 µm for ML141, all without significant effects on cell viability (Supplementary Figs. 5A, B, and C).
247 WB results indicated that the p65 and *MAPK/p38* pathways could impede the expression of tight
248 junction proteins (ZO-1, OCLN, and CLDN-5) following *M. bovis* infection (Figs. 4C and D).

249 To examine whether RBMX2 regulates cell adhesion ratio via p65 and MAPK/p38/JNK
250 pathways, we investigated the impact of *p65, p38* and *JNK* activators on cell adhesion in *RBMX2*
251 knockout EBL cells. Cell adhesion assays showed that treatment with p65 activator significantly
252 reduced cell adhesion ratio compared to the p38 and JNK activators (Figs. 4E and F).

253 To further substantiating the association between p65 and tight junction regulation in WT
254 EBL cells after *M. bovis* infection, we used siRNA to inhibit p65. WB analysis demonstrated that
255 siRNA significantly reduced p65 and *p-p65* expression (Figs. 4G and H). WB and
256 Immunofluorescence (IF) analyses revealed that suppressing p65 facilitated the expression of
257 ZO-1, OCLN, and CLDN-5 after *M. bovis* infection (Figs. 4G, H and I). Additionally, silencing p65 in
258 WT EBL cells inhibited the invasion of *M. bovis* into epithelial cells, as shown by plate counting
259 assay (Fig. 4J).

260 Finally, to investigate the relationship between *RBMX2*-mediated p65 and the findings above,
261 EBL cells were infected with *M. bovis* and *M. bovis* BCG. WB and high-content live imaging system

262 outcomes demonstrated diminished nuclear translocation of the p65 protein in *RBMX2* knockout
263 EBL cells compared with WT EBL cells (Figs. 4K and L).
264 In summary, our findings validate that *RBMX2* can regulate the phosphorylation and nuclear
265 translocation of p65 protein, leading to the degradation of tight junction proteins in EBL cells
266 infected with *M. bovis*.
267
268 ***RBMX2* promotes adhesion, invasion, and intracellular survival of pathogens**
269 Disrupting the intercellular tight junction barrier enhances bacterial adhesion and invasion [17,
270 18]. Based on these findings, we hypothesize that *RBMX2* may facilitates the adhesion and invasion
271 of *M. bovis* by degrading the tight junction proteins in EBL cells. To test this hypothesis, EBL cells
272 were infected with *M. bovis* at an MOI of 20:1, plate count assays indicated a significant
273 reduction in *M. bovis* adhesion in *RBMX2*-KO#17 and KO#23 EBL cells compared with WT EBL cells
274 (Fig. 4M) at 15 min, 30 min, 1 h, and 2 h post-infection (Fig. 4N). Furthermore, the invasion of *M.*
275 *bovis* in *RBMX2*-KO#17 and KO#23 EBL cells was decreased at 2, 4, and 6 h post-infection
276 compared with WT EBL cells. Additionally, the intracellular survival of *M. bovis* in *RBMX2*-KO#17
277 and KO#23 EBL cells was lower at 24, 48, 72 and 96 hpi compared with WT EBL cells (Fig. 4O).
278 Silencing *RBMX2* in human lung epithelial cells (H1299) also led to a significant reduction in the
279 adhesion, invasion, and intracellular survival of *M. bovis* (Figs. 4P-R). Thus, the host factor *RBMX2*
280 is critical for promoting the adhesion, invasion, and intracellular survival of *M. bovis*.
281 In addtion, pathway activators were employed to investigate the relationship between
282 pathway activation and the regulation of *M. bovis* adhesion and invasion by *RBMX2*. The results
283 showed that applying a p65 activator to *RBMX2* knockout EBL cells significantly impaired the tight
284 junction function of the epithelial barrier, thereby enhancing *M. bovis* adhesion and invasion in
285 EBL cells by regulating the phosphorylation and nucleation of p65 (Supplementary Figs. 6A and B).
286 Hence, RBMX2 promotes *M. bovis* adhesion and invasion in EBL cells by regulating the
287 phosphorylation and nucleation of p65
288 To further explore the influence of *RBMX2* on adhesion and invasion in the context of
289 different virulence *Mycobacterial* species, we utilized attenuated virulent *M. bovis* BCG and
290 *Mycobacterium smegmatis* (*M. smegmatis*) to infect EBL cells. The plate count assays revealed a

291 significant reduction in the adhesion of both *M. bovis* BCG and *M. smegmatis* in *RBMX2* knockout
292 EBL cells at various time points post-infection compared to WT EBL cells (Supplementary Figs. 6C
293 and D). Additionally, the invasion of *M. bovis* BCG and *M. smegmatis* was markedly diminished at
294 different hpi in *RBMX2* knockout EBL cells (Supplementary Figs. 6E and F). Consequently, the
295 virulence of *Mycobacterium* does not appear to affect the capacity of *RBMX2* to promote the
296 adhesion and invasion of *M. bovis* BCG and *M. smegmatis* in EBL cells.

297 Furthermore, we examined the role of *RBMX2* in regulating other bacteria associated with
298 bovine pneumonia by infecting EBL cells with *Salmonella* and *Escherichia coli* (*E. coli*). Our
299 findings indicated that *RBMX2* knockout EBL cells exhibited a degree of inhibition in bacterial
300 adhesion and invasion across all tested bacterial species compared to WT EBL cells
301 (Supplementary Figs. 6G-J).

302 In summary, our experiments provide compelling evidence that RBMX2 broadly promotes
303 the adhesion and invasion of pathogens associated with bovine pneumonia, highlighting its
304 potential as a target for developing disease-resistant cattle.

305

306 ***RBMX2* is highly expressed in lung cancer and regulates cancer-related metabolites**

307 Previous studies have demonstrated a link between bacterial infection and the initiation of
308 EMT [19-21]. Prolonged infection with *M. tb* or *M. bovis* induces oxidative stress, activates Toll-like
309 receptors (TLR), and elicits the release of inflammatory cytokines [22-24]. Consequently, this
310 phenomenon creates a favorable microenvironment for tumor development, progression, and
311 dissemination [25, 26]. Epidemiological investigations have established a correlation between TB and
312 the occurrence of lung cancer [27-30]. However, the precise cellular mechanism underlying this
313 association remain unclear.

314 In our research, we conducted a comprehensive analysis of gene families, revealing a
315 remarkable degree of *RBMX2* conservation among bovine, monkey, and human sources (Fig. 5A).
316 To further elucidate the involvement of *RBMX2* in cancer, we utilized the *TIMER2.0* database to
317 assess its expression patterns across various cancer types within The Cancer Genome Atlas
318 (TCGA). Our findings indicated a notable upregulation of *RBMX2* in lung cancer, specifically in
319 lung adenocarcinoma (LUAD) and lung squamous cell carcinoma (LUSC) (Fig. 5B).

320 To investigate the elevated expression of *RBMX2* in lung cancer further, we measured its
321 expression in both lung cancer epithelial cell lines and normal lung epithelial cell lines using
322 RT-qPCR. The results demonstrated that *RBMX2* expression in lung cancer epithelial cell lines
323 (NCIH1299, NCIH460, and CALU1) was significantly higher than that in normal lung epithelial cells
324 (BEAS-2B) (Fig. 5C). Additionally, immunofluorescence (IF) analysis revealed that *RBMX2*
325 expression levels were also higher in LUAD and LUSC tumor tissues compared to adjacent
326 non-cancerous lung tissues (Figs. 5D-F).
327 Furthermore, we investigate whether *RBMX2* regulates specific EMT-related metabolites to
328 mediate the EMT process in EBL cells following *M. bovis* infection. Our metabolomic analysis of
329 EBL cell samples at 48 hpi revealed that *RBMX2* knockout primarily enriched pathways related to
330 nucleotide metabolism, biosynthesis of cofactors, biosynthesis of nucleotide sugars, pentose and
331 glucuronate interconversions, vascular smooth muscle contraction, amino sugar, and nucleotide
332 sugar metabolism, chemokine signaling pathway, aldosterone synthesis and secretion, and
333 cGMP-PKG signaling pathway. Thes pathways are associated with tumor cells proliferation,
334 migration, and invasion (Fig. 5G). Differential metabolites are related to tumor metabolism,
335 mainly including 6-glucuronic acid estriol, adenosine, uridine 5 '- triphosphate, and 5' - deoxy-5 '-
336 (methylthio) (Figure 5H).
337
338 ***RBMX2* promotes the transformation of EBL cells from epithelial cells to mesenchymal**
339 **cells**
340 To investigate the association between *RBMX2* and EMT induced by *M. bovis*, we intially
341 infected EBL cells directly with *M. bovis*. This infection did not effectively induce the expression of
342 mesenchymal cell marker proteins (Supplementary Fig. 7A). Previous literature indicates that *M.*
343 *bovis* infection in macrophages, along with its secreted proteins, can stimulate the production of
344 cytokines such as TNF, IL-6, and TGF-β, all of which promote EMT process [31-34].
345 To further explore the impact of *M. bovis* infection on EMT progression in EBL cells, we
346 constructed a coculture model using *M. bovis*-infected BoMac cells (Fig. 6A and Supplementary
347 Fig. 7B). In this model, we identified EMT-related cytokines, including IL-6 and TNF, in *M.*
348 *bovis*-infected BoMac cells, revealing a significant increase compared to uninfected BoMac and

349 EBL cells (Fig. 6B). Notably, *RBMX2* expression was upregulated in EBL cells within this coculture
350 model following *M. bovis* infection (Fig. 6C).

351 We then examined the morphology changes in epithelial cells within the coculture model
352 using electron microscopy. The results demonstrated that most cells transitioned from circular to
353 an elongated morphology (Fig. 6D). Staining of the EBL cells cytoskeleton with ghost pen cyclic
354 peptide highlighted significant morphological alterations, with EBL cells transforming from
355 spherical to spindle-shaped (Supplementary Fig. 7C).

356 Additionally, we assessed the expression of EMT-related mRNAs and proteins in EBL cells
357 after coculture with *M. bovis-infected* BoMac cells. This analysis reveald a significant
358 downregulation of the epithelial cell marker protein *E-cadherin* and a notable upregulation of
359 mesenchymal markers *N-cadherin* and *MMP-9*, as determined by RT-qPCR and WB (Fig. 6E,
360 Supplementary Fig. 7D). The coculture with, *M. bovis-infected* BoMac cells enhanced the
361 migratory and invasive properties of EBL cells, as demonstrated by Transwell assay (Figs. 6F and
362 G).

363 To confirm the impact of *RBMX2* knockout on the EMT process in the coculture model, we
364 observed that *RBMX2* knockout cells exhibited significant upregulation of the epithelial cell
365 marker protein *E-cadherin* and downregulation of the mesenchymal cell marker *N-cadherin* and
366 *MMP-9* compared to WT EBL cells, as shown by RT-qPCR and WB (Fig. 6H and Supplementary Fig.
367 7E). Wound healing and Transwell assays demonstrated that the migration and invasion rates of
368 *RBMX2* knockout cells were markedly lower than those of WT EBL cells (Figs. 6I, J, and K).

369 Finally, we silenced RBMX2 in the human lung cancer epithelial cell line H1299, which
370 expresses high levels of RBMX2, to assess the effect on EMT-related proteins, as well as invasion
371 and migration ability following *M. bovis* infection. The results indicated that RBMX2 significantly
372 inhibited the EMT process in H1299 cells post-infection (Supplementary Figs. 8A and B).

373 In conclusion, we successfully established a coculture model involving *M. bovis*-infected
374 BoMac cells that induce EMT in EBL cells, thereby demonstrating that the host factor *RBMX2*
375 effectively promotes the EMT process in this context.

376

377 ***RBMX2* facilitates the EMT process via the *p65/MMP-9* pathway**

378 EMT enhances the migration and invasion capabilities of tumor cells [35-37]. Both p65 and
379 *MAPK/p38/JNK* pathways have been shown to regulate the EMT process through various
380 mechanisms. [38-41]. To elucidate the precise regulatory role of *RBMX2* in the EMT process within
381 the coculture model of EBL cells, we assessed the *MAPK* pathway and p65 protein levels via WB.
382 Our findings revealed a significant reduction in the phosphorylation of *p65* and *MAPK/p38/JNK* in
383 *RBMX2* knockout cells infected with *M. bovis,* compared to WT EBL cells (Supplementary Fig. 8C).
384 To determine the specific pathways regulating the EMT phenotype of p65 and
385 *MAPK/p38/JNK* in the coculture model, *RBMX2* knockout EBL cells were treated with *PMA*,
386 *Anisomysin*, and *ML141.* We observed that p65 downregulates the expression level of *E-cadherin*
387 while simultaneously upregulating *MMP-9* expression (Fig. 7A). The *MAPK/p38* pathway inhibits
388 *E-cadherin* expression while promoting *N-cadherin* expression. Conversely, the *MAPK/JNK*
389 pathway impedes *N-cadherin* expression while facilitate the expression of *E-cadherin and MMP-9*.
390 Furthermore, we comprehensively investigated the correlation between pathway activation and
391 the migration and invasion of phenotypes, demonstrating that the activation of the p65 pathway
392 enhances the migratory and invasive capabilities of EBL cells, as evidenced by the Transwell assay
393 (Figs. 7B and C) and wound-healing assay (Figs. 7D and E) .
394 Invasion and migration are critical stages in tumor development, influenced by
395 *p65*-dependent factors such as matrix metalloproteinases, urokinase fibrinogen activators, and
396 interleukin-8 [42-46]. To further substantiate the correlation between the p65 protein and the
397 regulation of the EMT process in EBL cells post-*M. bovis* infection, we employed siRNA to inhibit
398 p65 expression in WT EBL cells. This suppression was found to inhibit *MMP-9* expression, as
399 demonstrated by WB (Figs. 7F and G).
400 To verify the regulatory mechanism between *RBMX2* and *p65*, we first identified multiple
401 amino acid residues in the *RBMX2* promoter that form strong interactions through docking (Fig.
402 7H). Additionally, we queried the *RBMX2* promoter region for binding sites of the transcription
403 factor p65 using JASPAR data, subsequently validating this interaction using a dual luciferase
404 reporter plasmid system (Fig. 7I) and Chip-PCR (Fig. 7J). Notably, *RBMX2* and p65 exhibited
405 multiple amino acid residues forming strong bonds in protein docking, yielding a docking score of
406 1978.643 (Fig. 7K).

407 Moreover, MMP-9 is known to induce EMT in epithelial cells, enhancing their invasiveness.
408 The regulatory mechanisms involving p65 and *MMP-9* have been documented in several studies
409 [47, 48]. In our research, we identified multiple binding sites in the promoter sequences of p65 and
410 MMP-9 through molecular docking (Fig. 7L) and confirmed the biding site between *MMP-9*
411 promoter and *p65* protein via Chip-PCR (Fig. 7M). Using protein docking, we validated the
412 relationship between bovine p65 protein and MMP-9, with a binding score of 1784.378 (Fig. 7N).
413 In summary, *RBMX2* facilitates the EMT process of EBL cells following *M. bovis* infection by
414 activating the *p65/MMP-9* pathway.
415
416 **Discussion**
417 The resurgence of *M. bovis*-associated TB presents a substantial global challenge, affecting
418 both livestock and human populations. Notably, *M. bovis* exhibits over 99% nucleotide similarity
419 with *M. tb* [49]. The pathogenesis of TB is complex process influenced by a confluence of bacterial,
420 host, and environmental factors. Both *M. tb* and *M. bovis* have evolved sophisticated strategies to
421 evade host immune responses, enabling their long-term intracellular persistence. It is estimated
422 that approximately one-third of the global population harbors latent TB infections [50, 51].
423 The successful establishment of infection by mycobacteria is contingent upon their ability to
424 circumvent early innate immune defenses, employing both transcriptional and
425 post-transcriptional regulatory strategies within host macrophages [52-56]. Despite notable
426 advancements in the field, unraveling the mechanisms of immune evasion and understanding the
427 dynamics of latent infections caused by *M. tb* and *M. bovis* remains a substantial challenge. The
428 cellular immune response to these pathogens is inherently complex, further compounded by the
429 microdiversity of mycobacteria within individual hosts and the variability of immune responses
430 among different individuals [54, 57].
431 Lung epithelial cells serve as the primary physical barrier against infection and play a pivotal
432 role in the innate immune response. These cells not only function as a frontline defense but also
433 recruit and activate antigen-presenting cells, such as macrophages, to initiate adaptive immune
434 responses against *M. bovis* infection [58, 59]. Given that alveolar epithelial cells can act as reservoirs
435 for *M. bovis*, their role in the infection process is particularly significant. Additionally, activated

436 macrophages and neutrophils enhance the bactericidal effects of alveolar epithelial cells, further
437 contributing to the host's defense mechanisms [60, 61].

438 In our study, we utilized a CRISPR-Cas9 mutant library developed in our laboratory to
439 investigate potential host factors influencing M. bovis infection. Notably, we identified *RBMX2* as
440 a protein with significant anti-*M. bovis* infection capabilities. The *RBMX2* protein, characterized
441 by an RNA recognition motif within its 56-134 amino acid residue region, is implicated in mRNA
442 splicing through spliceosomes and is emerging as a potential molecular marker for sperm activity.
443 [62]. The downregulation of RBMX2 in the X chromosome of lung telocytes suggests its involvement
444 in cellular immunity [63].

445 Further exploration of RBM genes in cattle revealed that EIF3G, RBM14, RBM42, RBMX44,
446 RBM17, PUF60, SART3, and RBM25 belong to the same subfamily as RBMX2. Previous studies
447 have demonstrated that genes within this subfamily can regulate the proliferation and lifecycle of
448 cancer cells. For instance, EIF3G modulates the mTOR signaling pathway, inhibiting the
449 proliferation and metastasis of bladder cancer cells [64]. Similarly, RBM14 has been linked to the
450 reprogramming of glycolysis in lung cancer, acting as a novel epigenetically activated oncogene [60].
451 Despite these insights, the specific function of RBMX2 in the context of *M. bovis* infection and its
452 potential role in cancer pathogenesis remain largely unexplored.

453 Our findings reveal that RBMX2 is upregulated in TB-infected cells and tissues,
454 demonstrating the capacity to inhibit *M. bovis* invasion. Transcriptomic analyses indicate that
455 RBMX2 may disrupt tight junctions within epithelial cells and promote epithelial-mesenchymal
456 transition (EMT) following *M. bovis* infection.

457 Our findings reveal that *RBMX2* is upregulated in TB-infected cells and tissues,
458 demonstrating its capacity to inhibit *M. bovis* invasion. Transcriptomic analyses suggest that
459 *RBMX2* may disrupt tight junctions within epithelial cells and promote EMT following *M. bovis*
460 infection.

461 Epithelial cells serve as more than passive barriers; they actively participate in innate
462 immunity by regulating cytokine secretion and maintaining barrier integrity [61]. Disruptions in
463 epithelial tight junctions, often exacerbated by pro-inflammatory stimuli from pathogenic
464 bacteria, can facilitate bacterial translocation and subsequent infection [61 65, 66]

465 In our experiments, we observed that the disruption of the epithelial barrier facilitated *M.*
466 *bovis* adhesion and invasion. Conversely, the knockout of RBMX2 stabilized the epithelial barrier,
467 attenuating *M. bovis* invasion and intracellular survival. This stabilization also mitigated
468 downstream innate immune responses, reducing cellular inflammation, ROS production, and
469 apoptosis.

470 The loss of tight junction integrity is a precursor to EMT, a process increasingly recognized
471 for its role in cancer progression [20, 65-67]. Recent studies have established a link between bacterial
472 infections and EMT induction, particularly in the context of gastric adenocarcinomas [68, 69].
473 Epidemiological evidence suggests that TB may serve as a risk factor for lung cancer [70, 71];
474 however, the underlying cellular mechanisms remain elusive. Chronic TB infection has been
475 implicated in lung carcinogenesis, with reports indicating that BCG vaccination can enhance the
476 survival of tumor cells under inflammatory conditions [72 73].

477 Moreover, *M. tb*-infected THP-1 cells have been shown to induce EMT in lung
478 adenocarcinoma epithelial cells [74]. Chronic infection with *M. tb* is associated with oxidative stress
479 and inflammatory cytokine production, fostering an environment conducive to tumor progression
480 [75, 76]. Our analysis of RBMX2 across various cancers revealed increased expression levels in lung
481 adenocarcinoma (LUAD) and lung squamous cell carcinoma (LUSC), suggesting a conserved role in
482 tumor biology across species.

483 In light of these findings, we constructed a model of *M. bovis* infection in EBL cells to
484 investigate EMT induction. Initial results indicated that *M. bovis* alone did not induce EMT;
485 however, a co-culture model incorporating *M. bovis*-infected BoMac cells successfully induced
486 EMT in EBL cells. Notably, the knockout of RBMX2 in this context inhibited EMT, suggesting that
487 RBMX2 may elevate the risk of lung cancer through EMT induction following *M. bovis* infection.

488 In conclusion, our study identifies *RBMX2* as a novel host factor influencing susceptibility to
489 *M. bovis* infection, playing a crucial role in both TB pathogenesis and the EMT process associated
490 with lung cancer. Targeting RBMX2 may present a promising avenue for the prevention and
491 treatment of TB in both humans and animals. Additionally, the effective modulation of *RBMX2*
492 could potentially mitigate the incidence of TB-associated EMT and its implications for lung cancer
493 development in the near future.

494 **Conclusion**

495 Our findings demonstrate that *RBMX2* significantly facilitates the invasion of *M. bovis* by
496 promoting the activation of the p65 protein. This activation undermines the integrity of the
497 epithelial cell barrier and promotes the EMT of epithelial cells through the *p65/MMP-9* signaling
498 pathway. These insights elucidate the critical role of RBMX2 in *M. bovis* pathogenesis and
499 highlight its potential as a therapeutic target for mitigating infection-related complications.

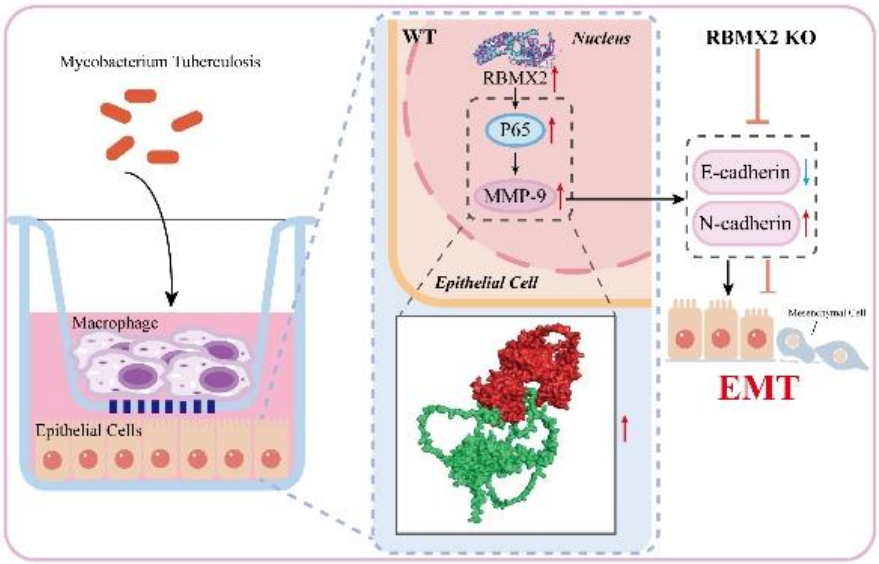

500
501
502

503 **Methods**

504 Patients and lung tissues

505 This study was approved by the Ethics Committee of Inner Mongolia Autonomous Region
506 People's Hospital, and written informed consent was obtained from all participating patients
507 (Approval Number: No. 2020021). A total of 35 specimens of lung cancer tissue, along with
508 adjacent normal lung tissue, were collected. We randomly selected the above specimens,
509 including age and gender. All patients involved in this study had not received any medication,
510 chemotherapy, or radiation therapy prior to surgical resection. The samples were subsequently
511 prepared for immunohistochemistry (IHC) and fluorescence in situ hybridization (FISH) assays.

512 Bovine clinical tissues

513 This project has received approval from the Experimental Animal Ethics Center of Huazhong
514 Agricultural University (Approval Number: HZAUCA-2024-0014). Following examination by

515 researchers at the National Animal Tuberculosis Professional Laboratory (Wuhan), bovine
516 tuberculosis tissue samples were collected from the lungs and livers of slaughtered cattle, with
517 each specimen measuring at least 5 cm × 5 cm × 5 cm and specifically including tissues exhibiting
518 tuberculous lesions.
519
520 Cell lines
521 EBL and 293T RRID:CVCL_0063 cells were generously provided by M. Heller from
522 Friedrich-Loeffler-Institute. These cells were cultured in heat-inactivated 10% fetal bovine serum
523 supplemented with Dulbecco's modified Eagle medium (DMEM, Gibco, USA) at 37°C and 5% CO_2
524 [77]. BoMac cells were kindly provided by Judith R. Stabel from the Johne's Disease Research
525 Project at the United States Department of Agriculture in Ames, Iowa, and were maintained
526 according to previously established protocols [78]. BoMac cells were grown in heat-inactivated 10%
527 fetal bovine serum supplemented with Roswell Park Memorial Institute 1640 (RPMI 1640, Gibco,
528 USA) at 37°C and 5% CO_2. Bovine lung alveolar primary cells were isolated in our laboratory and
529 cultured in heat-inactivated 10% fetal bovine serum supplemented with DMEM (Gibco, USA) at
530 37°C and 5% CO_2. BEAS-2B RRID:CVCL_0168, NCIH1299, NCIH460 RRID:CVCL_0459, and CALU1
531 epithelial cells were all provided by Professor Shi Lei from Lanzhou University, and all culture
532 procedures were conducted according to standardized protocols. We conduct regular testing on
533 all cell lines to eliminate contamination from mycoplasma and black fungus.
534
535 Bacterium
536 *M. bovis* (ATCC:19210), originally isolated from a cow, is maintained in this laboratory. *M.*
537 *smegmatis* mc^2155 (NC_008596.1) and *M. bovis* BCG-Pasteur (ATCC:35734) were generously
538 provided by Professor Luiz Bermudez from Oregon State University. All strains were cultured in a
539 Middlebrook 7H9 broth (BD, MD, USA) supplemented with 0.5% glycerol (Sigma, MO, USA), 10%
540 oleic acid–albumin–dextrose–catalase (OADC, BD, USA) and 0.05% Tween 80 (Sigma, MO, USA) or
541 on Middlebrook 7H11 agar plates (BD, MD, USA) containing 0.5% glycerol (Sigma, MO, USA) and
542 10% OADC (BD).
543 Prior to infection, the optical densities of bacterial cultures at 600 nm (OD600) were

544 adjusted to the required MOI using the standard turbidimetric card. The cultures were then
545 centrifuged at 3,000 g for 10 min. The precipitated bacteria were resuspended in medium and
546 dispersed using an insulin syringe. Subsequently, 50 μL of 10-fold serially diluted bacterial
547 suspension was plated onto Middlebrook 7H11 agar to determine the number of viable bacteria
548 (colony-forming units, CFUs). All experiments involving *M. bovis* were conducted in strict
549 accordance with the biosafety protocols established for the Animal Biosafety Level 3 Laboratory
550 of the National Key Laboratory of Agricultural Microbiology at Huazhong Agricultural University.
551 *E. coli* (ATCC:25922) was donated by Professors Zhou Rui and Wang Xiangru of Huazhong
552 Agricultural University, while *Salmonella* (ATCC:14028) has been preserved and passed down
553 through generations in our laboratory. These strains were resuscitated, and single colonies were
554 purified, cultured, and grown in Luria–Bertani broth.
555
556 Generation of the *RBMX2*-KO EBL cells
557 The small guide RNA (sgRNA) sequence targeting the bovine *RBMX2* gene (5'-
558 GAATGAGCGTGAGGTCGAAC-3') was cloned into the pKLV2-U6gRNA5 (BbsI)-PGKpuro2ABFP
559 (#67991), kindly provided by Professor Zhao Shuhong of Huazhong Agricultural University, to
560 construct the recombined lentivirus. EBL cells were then infected with either the *RBMX2* pKLV2-
561 U6gRNA5(BbsI)-PGKpuro2ABFP (#67991) lentivirus or the empty vector pKLV2-U6gRNA5(BbsI)-
562 PGKpuro2ABFP (#67991) lentivirus as a negative control. After 48 to 60 hpi, puromycin (2.0
563 mg/mL) was added to select the positive clones. Finally, the monoclonal cells obtained through
564 limiting dilution were expanded, and the knockout of RBMX2 was confirmed via PCR assay
565 (Table S1).
566 Table S1

sgRNA	sequence
sgRNA-F	5'-CCTTGCCCAATTTTTCGGAGG-3'
sgRNA-R	5'-ACAGGAGGATGGTAGTAACGG-3'

567
568
569 Extraction of total RNA and RT-qPCR

570 Cold phosphate-buffered saline (PBS, HyClone, China) was used to wash the cells three times,
571 after which 1 mL of Trizol (Invitrogen, USA) was added per well to lyse the cells. The lysate was
572 collected in EP tubes, and 200 μL of chloroform was subsequently added. The mixture was
573 vortexed for 30 seconds and then centrifuged at 12,000 rpm for 10 minutes at 4°C. Following
574 centrifugation, 500 μL of the supernatant was transferred to a new EP tube. To this supernatant,
575 500 μL of isopropanol was added and mixed gently by inversion. The mixture was allowed to
576 stand for 10 minutes at 4°C before being centrifuged again at 12,000 rpm for 15 minutes at 4°C.
577 The supernatant was discarded, revealing the RNA pellet. Next, the RNA pellet was washed with
578 1 mL of 75% ethanol and centrifuged at 7,500 rpm for 5 minutes at 4°C. The supernatant was
579 removed, and the RNA pellet was air-dried for 15 minutes. Subsequently, 20 μL of DEPC-treated
580 water was added, and the mixture was incubated at 58°C in a water bath for 10 minutes to
581 dissolve the RNA. Purified RNA was then obtained.
582 To assess RNA purity, the OD260/OD280 ratio was measured using a NanoDrop ND-1000
583 instrument (Agilent Inc., USA), with values between 1.8 and 2.0 indicating acceptable purity. RNA
584 integrity and potential contamination with genomic DNA were evaluated using denaturing
585 agarose gel electrophoresis. The samples were stored at -80°C for later analysis.
586 Reverse transcription of the RNA samples was performed using HiScript III RT SuperMix for
587 qPCR (+gDNA wiper, Vazyme, China). Four microliters of 4× gDNA wiper mix were added to 1 μg
588 of RNA, followed by the addition of 16 μL of RNase-free ddH2O. The mixture was incubated at
589 42°C for 2 minutes to eliminate genomic DNA. Reverse transcription was subsequently carried
590 out by adding 4 μL of 5× HiScript III qRT SuperMix, with the mixture incubated at 37°C for 15
591 minutes and then at 85°C for 5 seconds to synthesize cDNA.
592 cDNA expression across different sample groups was quantified using AceQ qPCR SYBR
593 Green Master Mix (Vazyme, China) in a ViiA7 real-time PCR machine (Applied Biosystems Inc.,
594 USA). The final volume of each real-time PCR reaction was 20 μL, comprising 10 μL of 2× AceQ
595 qPCR SYBR Green Master Mix, 0.4 μL of upstream primer (10 μM), 0.4 μL of downstream primer
596 (10 μM), 0.4 μL of 50× ROX reference dye 2, 3 μL of cDNA template, and 5.8 μL of ddH_2O. The PCR
597 conditions were as follows: 95°C for 5 minutes (1 cycle), 95°C for 10 seconds (40 cycles), and 60°C
598 for 30 seconds (40 cycles). The primer sequences for RT-qPCR are provided in Table S2.

599 Table S2

Number	Primer	Sequence
1	Bovine-β-actin-F	5′-AGCAAGCAGGAGTACGATGAG-3′
2	Bovine-β-actin-R	5′-ATCCAACCGACTGCTGTCA-3′
3	Human-β-actin -F	5′- CACCATTGGCAATGAGCGGTTC-3′
4	Human-β-actin -R	5′- AGGTCTTTGCGGATGTCCACGT-3′
5	Bovine-RBMX2-F	5′-TCCCACCGGCACAAAAAGTC-3′
6	Bovine-RBMX2-R	5′-TCAGTGATACCTGAGCTCCC-3′
7	Human-RBMX2-F	5′-ACCCCCTCACCAAGTTTGTC-3′
8	Human-RBMX2-R	5′-GTGCTTCTTAGGGCCAGTGT-3′
9	Bovine-HSPB8-F-1	5′-GACCAAGGACGGATACGTGG-3′
10	Bovine-HSPB8-R-1	5′-AGTTCTTGGAGACGATGCCC-3′
11	Bovine-ST14-F-1	5′-CTCGGCGCTGGATTCAAGTA-3′
12	Bovine-ST14-R-1	5′-CAAGAACTCCACGCCTTCCT-3′
13	Bovine-MUC16-F-1	5′-TGTGCATGTGACAGCAGAGC-3′
14	Bovine-MUC16-R-1	5′-CTGGAAACTGGGAGTGGTCG-3′
15	Bovine-TNC-F-1	5′-TGGCATCGGAGAATGCCTTT-3′
16	Bovine-TNC-R-1	5′-CAGCTTCCTCTGGGTTCCTG-3′
17	Bovine-GPX2-F-1	5′-ACCCGTTTTCCCTCATGACC-3′
18	Bovine-GPX2-R-1	5′-CGGCCCAATGAGGAACTTCT-3′
19	Bovine-THBS2-F-1	5′-GGGGACGCTTGTAAAGACGA-3′
20	Bovine-THBS2-R-1	5′-AATCTGAGTGGTGCCCTTGG-3′
21	Bovine-IL-7-F-1	5′-GCAATTGCCTGAATAACGAACCT-3′
22	Bovine-IL-7-R-1	5′-TTACCCTTGCTGGTGCAGTT-3′
23	Bovine-IL-24-F-1	5′-GACGCCTGCCCAACTTTCTT-3′
24	Bovine-IL-24-R-1	5′-AAGGGATGCTTGAGGGCTTG-3′
25	Bovine-FRMD4B-F-1	5′-CAGAGACAGGAGCACCAAGG-3′
26	Bovine-FRMD4B-R-1	5′-TTAAACTGCCGTTGCTTGCC-3′

27	Bovine-OMD-F-1	5′-GCTCAACGTTGGACACAACA-3′
28	Bovine-OMD-R-1	5′-AGCTTATTGGCGCTTTCAGC-3′
29	Bovine-NOS3-F-1	5′-GTTCCCTCGCGTGAAGAACT-3′
30	Bovine-NOS3-R-1	5′-CTGGTTGATGAAGTCCCTGGC-3′
31	Bovine-MCTP1-F-1	5′-AGTTCCGACTTGGGCATCAG-3′
32	Bovine-MCTP1-R-1	5′-TACTGAGAGCCGACAGGTCA-3′
33	Bovine-MFAP5-F-1	5′-TGATATCCAGCCTTCCACCG-3′
34	Bovine-MFAP5-R-1	5′-CCGATGCACGGAGTAGAGTC-3′
35	Bovine-MMP-9-1-F	5′-CGCTATGGCTACACTCCTGG-3′
36	Bovine-MMP-9-1-R	5′-TGAGTTCGCCCTCAAAGGTC-3′
37	Bovine-N-cadherin-1-F	5′-CACTGCGATTGATGCTGACG-3′
38	Bovine-N-cadherin-1-R	5′-TGCCACCGTGATAATGTCCC-3′
39	Bovine-E-cadherin 1-F	5′-CAGAAGATGACACCCGGGAC-3′
40	Bovine-E-cadherin 1-R	5′-AGCATCCAGGCCCCTATGTA-3′
41	Bovine-CLDN-5-F-1	5′-CCTGGACCACAACATCGTGA-3′
42	Bovine-CLDN-5-R-1	5′-GGAGTCGTACACCTTGCACT-3′
43	Bovine-OCLN-F-1	5′-CTTTCAAAAAGGGCTCCCGC-3′
44	Bovine-OCLN-R-1	5′-TGGATATTCCCTGATCCAGTCG-3′
45	Bovine-TJP1-F-1	5′-CTCAAGTTCCTGAAGCCCGT-3′
46	Bovine-TJP1-R-1	5′-TAGGATCACCCGACGAGGAG-3′
47	Bovine-TNF-F-1	5′-GAAGTTGCTTGTGCCTCAGC-3′
48	Bovine-TNF-R-1	5′-AACCAGAGGGCTGTTGATGG-3′
49	Bovine-IL-6-F-1	5′-CTTCTGCTTTCCCTACCCCG-3′
50	Bovine-IL-6-R-1	5′-TTCTGCCAGTGTCTCCTTGC-3′
51	Bovine-IL-1β-F-1	5′-AAAAGCTTCAGGCAGGTGGT-3′
52	Bovine-IL-1β-R-1	5′-AACTCGTCGGAGGACGTTTC-3′

602 Western blot

603 RIPA reagent (Sigma, USA), supplemented with protease inhibitors and phosphatase
604 inhibitors (Roche, China), was added to the cell samples, and the cells were lysed on ice for 30
605 minutes. The supernatant was collected by centrifugation at 12,000 rpm and 4°C for 10 minutes.
606 Protein concentrations of each sample were determined using a BCA kit (Beyotime, China), and
607 the proteins were adjusted to equal concentrations.

608 The protein samples were mixed with 5× protein loading buffer and boiled for 10 minutes.
609 Proteins were then separated using SDS-PAGE on 10% polyacrylamide gels at 100 V for 90
610 minutes, followed by transfer to polyvinylidene difluoride (PVDF) membranes (Millipore,
611 Germany) at 100 V for 70 minutes. The PVDF membrane was incubated in 5% skimmed milk for 4
612 hours to block non-specific binding. The membrane was washed three times with Tris-buffered
613 saline containing 0.15% Tween-20 (TBST) for 5 minutes each.

614 Subsequently, the membrane was incubated with a primary antibody at 4°C for 12 hours,
615 followed by a secondary antibody at room temperature for 1 hour. The following primary
616 antibodies were utilized: ZO-1 (Bioss, China), OCLN (Proteintech, China), CLADN-5 (Proteintech,
617 China), MMP-9 (Proteintech, China), E-cadherin (Proteintech, China), N-cadherin (Bioss, China),
618 LaminA/C (Proteintech, China), β-actin (Bioss, China), p65 (CST, USA), p-p65 (CST, USA), and a
619 MAPK-related antibody (CST, USA). The following secondary antibodies were used: anti-mouse
620 HRP secondary antibody and anti-rabbit HRP (Invitrogen, USA).

621

622 Phylogenetic tree construction and gene structure and function predictive analysis of the
623 bovine RBM family

624 The bovine RBM protein sequences were converted into FASTA format files and imported
625 into MEGA-X for comparative analysis. The neighbor-joining method was employed to construct
626 the phylogenetic tree of the CsGRF protein. The iTOL website (https://itol.embl.de/) was utilized
627 to enhance the visualization of the CsGRF phylogenetic tree. Additionally, the MEME Suite
628 database (http://meme-suite.org/) was used for the online analysis of conserved motifs within
629 the RBM gene family.

630

631 Adhesion assay

632 EBL cells were infected with different live bacteria at an MOI of 20 for durations of 15
633 minutes, 30 minutes, 1 hour, and 2 hours at 4°C. Following infection, the cells were washed three
634 times with phosphate-buffered saline (PBS; Gibco, USA) to remove any extracellular bacteria.
635 After thorough washing, cell lysis was achieved using 0.1% Triton X-100 (Beyotime, China). The
636 resulting cell lysates were plated onto 7H11 or LB agar plates and incubated for several days to
637 facilitate colony-forming unit (CFU) enumeration.

638

639 Invasion assay

640 EBL cells were infected with various live bacteria at an MOI of 20 for durations of 2, 4, and 6
641 hours at 37°C. Following infection, gentamycin (Procell, China) was added at a concentration of
642 100 μg/mL for 2 hours to eliminate any extracellular bacteria. The infected cells were then
643 washed three times with phosphate-buffered saline (PBS) (Gibco, USA) to remove remaining
644 extracellular bacteria. After sufficient washing, the cells were lysed using 0.1% Triton X-100
645 (Beyotime, China). The resulting cell lysates were subsequently plated onto 7H11 or LB agar
646 plates and incubated for several days to allow for colony-forming unit (CFU) enumeration.

647

648 Intracellular survival assay

649 EBL cells were infected with various live bacteria at an MOI of 20 for 6 hours at 37°C.
650 Following infection, gentamycin (Procell, China) was added at a concentration of 100 μg/mL to
651 eliminate extracellular bacteria for 2 hours. The infected cells were then washed three times with
652 phosphate-buffered saline (PBS) (Gibco, USA) to remove any remaining extracellular bacteria,
653 which is referred to as the 0-hour time point.

654 Subsequently, the infected cells were cultured in complete medium supplemented with
655 Triton X-100 (0.1%) (Beyotime, China) at various time points: 0, 24, 48, and 72 hours hpi. Cell
656 lysates were plated onto 7H11 or LB agar plates and allowed to incubate for several days to
657 facilitate colony-forming unit (CFU) counting.

658

659

660 RNA-Seq, proteomics and metabolomics

661 Total RNA was isolated using Trizol Reagent (Invitrogen Life Technologies), and the
662 concentration, quality, and integrity were determined using a NanoDrop spectrophotometer
663 (Thermo Scientific). Three micrograms of RNA were used as input material for RNA sample
664 preparation. Sequencing libraries were generated according to the following steps: mRNA was
665 purified from total RNA using poly-T oligo-attached magnetic beads. Fragmentation was
666 performed using divalent cations under elevated temperature in an Illumina proprietary
667 fragmentation buffer. First-strand cDNA was synthesized using random oligonucleotides and
668 Super Script II. Second-strand cDNA synthesis was subsequently performed using DNA
669 Polymerase I and RNase H. The remaining overhangs were converted into blunt ends via
670 exonuclease/polymerase activities, and the enzymes were removed. After adenylation of the 3'
671 ends of the DNA fragments, Illumina PE adapter oligonucleotides were ligated for hybridization.
672 To select cDNA fragments of the preferred length of 400–500 bp, the library fragments were
673 purified using the AMPure XP system (Beckman Coulter, Beverly, CA, USA). DNA fragments with
674 ligated adaptor molecules at both ends were selectively enriched using the Illumina PCR Primer
675 Cocktail in a 15-cycle PCR reaction. The products were purified (AMPure XP system) and
676 quantified using the Agilent high-sensitivity DNA assay on a Bioanalyzer 2100 system (Agilent).
677 The sequencing library was then sequenced on the NovaSeq 6000 platform (Illumina) by
678 Shanghai Personal Biotechnology Co., Ltd.

679 RNA sequencing services were provided by Personal Biotechnology Co., Ltd. Shanghai, China.
680 The data were analyzed using the free online platform Personalbio GenesCloud
681 (https://www.genescloud.cn). Proteomics and metabolomics were performed by METWARE.

682

683 Differential expression analysis of the transcriptome

684 HTSeq (0.9.1) RRID:SCR_005514 statistical methods were employed to compare the read
685 count values for each gene, which served as the original expression measurements, while FPKM
686 was utilized for normalization. Subsequently, differential gene expression was analyzed using
687 DESeq (1.30.0) RRID:SCR_000154 under the following screening criteria: a fold change of
688 |log2FoldChange| > 2 and a significant P-value < 0.05. We employed the R language Pheatmap

689 (1.0.8) software package to conduct bidirectional clustering analysis of all differentially expressed
690 genes across samples. A heatmap was generated based on the expression levels of the same
691 gene in various samples and the expression patterns of different genes within the same sample,
692 utilizing the Euclidean method for distance calculation and the complete linkage method for
693 clustering. Data analysis was performed using the free online platform Personalbio GenesCloud
694 (https://www.genescloud.cn).
695
696 GO and KEGG enrichment analysis
697 We mapped all genes to terms in the Gene Ontology (GO) database and calculated the
698 number of differentially enriched genes for each term. GO enrichment analysis was conducted on
699 the differentially expressed genes using the topGO package, where P-values were determined
700 using the hypergeometric distribution method. A threshold of P-value < 0.05 was set to identify
701 significant enrichment, allowing us to pinpoint GO terms associated with significantly enriched
702 differential genes and to elucidate the primary biological functions they perform. Additionally, we
703 employed ClusterProfiler (3.4.4) software to conduct KEGG pathway enrichment analysis for the
704 differential genes, concentrating on pathways with a P-value < 0.05. The data analysis was carried
705 out using the free online platform Personalbio GenesCloud (https://www.genescloud.cn).
706
707 Flow cytometry assay
708 Cells were washed with cold PBS and then centrifuged at 1,500 rpm for 5 minutes; the
709 supernatant was discarded. The cells were fixed in 70% ethanol for 12 hours. Following fixation,
710 the cells were centrifuged again at 1,500 rpm for 5 minutes, and the supernatant was removed.
711 The cells were washed once with cold PBS.
712 For staining, a Cell Cycle and Apoptosis Analysis Kit (Beyotime, China) was utilized. The
713 staining mixture was prepared with a total volume of 535 μL, comprising 500 μL of staining buffer,
714 25 μL of PI dye, and 10 μL of RNase A. The samples were incubated with the staining mixture at
715 37°C for 30 minutes prior to detection.
716
717 Cell viability assay

718 EBL cells were infected with *M. bovis* at an MOI of 100. Cell viability was assessed at 48, 72,
719 96, 120, and 144 hpi using the CCK-8 assay (Dojindo, Kumamoto, Japan).
720 At each time point, fresh medium containing 10% CCK-8 was added to a 96-well cell plate
721 and incubated for 60 minutes at 37°C. The cell viability was then determined by measuring the
722 absorbance at 450 nm. The percentage of cell viability was calculated using the following
723 formula:
724 cell viability (%) = [A (infection group) − A (blank group)] / [A (infection group) A (blank
725 group)] × 100
726
727 Wound-healing assay
728 Approximately 2×10^5 treated cells were added to a 6-well plate after EBL cells were
729 cocultured with BoMac cells for 48 hours following *M. bovis* infection and subsequently digested
730 with 1× trypsin. Once the cells were evenly spread, a cross was drawn along a ruler using a 200 µL
731 pipette tip to create a wound.
732 The cells were washed three times with PBS (Gibco, USA) to remove any detached cells, and
733 serum-free medium was added to each well. Images were taken at 0, 12, and 24 hours of culture,
734 and the healing rate was calculated using ImageJ software.
735
736 Cell adhesion assay
737 To assess the level of cell adhesion between RBMX2 knockout and wild-type (WT) EBL cells
738 after *M. bovis* infection, a cell adhesion assay was performed using a cell adhesion detection kit
739 (Bestbio, China) according to the manufacturer's protocol. Matrigel (20 mg/L) was added to a
740 96-well plate at 100 µL per well. Subsequently, 3×10^4 cells were added to the adhesion plate and
741 incubated in a CO2 incubator for 6 hours. After incubation, the wells were washed twice with PBS,
742 and the adhered cells were stained with 10 µL of cell stain solution A for 2 hours at 37°C. The
743 level of cell adhesion was quantified by measuring the absorbance at 560 nm.
744
745 Transwell assay
746 5×10^4 treated cells and 200 µL of serum-free medium were added to each upper chamber of

747 a Transwell (Corning, USA), while 550 μL of complete medium was added to the lower chamber.
748 The cells were incubated for 24 hours.

749 The following day, the upper chamber was removed, and 550 μL of 4% paraformaldehyde
750 (Beyotime, China) was added for 30 minutes. After fixation, 550 μL of crystal violet dye (Beyotime,
751 China) was added to each well for another 30 minutes. The upper chamber was then washed
752 with PBS for 30 seconds and dried upside down with a cotton swab.

753 After drying, the membrane of the chamber was removed and placed on a glass slide,
754 followed by the addition of a neutral gum seal. Three random fields of view were selected under
755 the microscope for imaging, and the cell count was performed using ImageJ RRID:SCR_003070
756 software.

757

758 Crystal violet staining assay

759 EBL cells were infected with *M. bovis* at an MOI of 100. The surviving cells on six-well plates
760 were then fixed with 4% paraformaldehyde (Beyotime, China). After fixation, the cells were
761 stained with 0.1% crystal violet staining solution (Beyotime, China) and rinsed five times with PBS
762 (Gibco, USA). The plates were placed in a 37°C oven for 6 hours before being photographed.

763

764 *M. bovis* infection of BoMac and coculture with EBL cells

765 BoMac cells were seeded into the upper chamber of a 0.4 μm pore size Transwell (Corning,
766 USA) at a density of 3×10^4 cells per insert in RPMI 1640 medium supplemented with 10% FBS.
767 The following day, the cells were infected with *M. bovis* at an MOI of 5 for 4 hours. After infection,
768 the cells were washed three times with 1× warm PBS and treated with Gentamycin (100 μg/mL)
769 for 2 hours to eliminate any extracellular bacilli.

770 The infected and uninfected BoMac cells were then incubated for 24 hours to mitigate the
771 effects of *M. bovis* infection. Afterward, the cells underwent an additional 24-hour incubation
772 period in fresh RPMI 1640 medium before coculturing with EBL cells.

773 In parallel, EBL cells were seeded at a density of 2×10^5 cells per well onto 12-well plates
774 containing DMEM supplemented with 10% FBS. The following day, culture inserts containing
775 either *M. bovis*-infected or uninfected BoMac cells were introduced into the wells of the 12-well

776 plates containing EBL cells, and the coculture was incubated for up to 24 and 48 hours in
777 serum-free DMEM.
778
779 Small interfering RNA (siRNA) transfection
780 EBL cells were transfected with p65 siRNA (Tsingke, China) using jetPRIME (Polyplus, France)
781 following the manufacturer's instructions. Scrambled siRNA (Tsingke, China) served as a negative
782 control.
783 Cells were seeded in 12-well plates and cultured at 37°C in a 5% CO_2 atmosphere. To prepare
784 the transfection mixture, 0.8 μg of jetPRIME was incubated with 1 μL of siRNA for 10 minutes.
785 This mixture was then added to the cells and incubated for 12 hours.
786 Following the incubation, RNA extraction was performed, and the efficiency of transfection
787 was calculated.
788 The siRNA sequences used were as follows:
789 Cattle p65-1 siRNA, sense 5'-GCAGUUUGAUACCGAUGAA (dT)(dT)-3';
790 Cattle p65-1 siRNA, antisense 5'-UUCAUCGGUAUCAAACUGC (dT)(dT)-3';
791 Cattle p65-2 siRNA, sense 5'-GGACGUACGAGACCUUCAA (dT)(dT)-3';
792 Cattle p65-2 siRNA, antisense 5'-UUGAAGGUCUCGUACGUCC (dT)(dT)-3'.
793
794 P65 nuclear translocation assay
795 For the p65 nuclear translocation assay, RBMX2 knockout and wild-type cell lines were
796 transfected with the pCMV-EGFP-p65 plasmid. Following transfection, bovine lung epithelial cells
797 were infected with *M. bovis*.
798 After infection, the cell nuclei were stained with Hoechst dye. The entry of p65 into the
799 nucleus was analyzed at different time points using a confocal high-resolution cell imaging
800 analysis system from PerkinElmer Life and Analytical Sciences Ltd. (Britain). This imaging
801 technique allowed for the assessment of p65 translocation into the nucleus in response to
802 infection.
803
804 CHIP-PCR

805 Formaldehyde cross-linking and ultrasonic fragmentation of cells were performed. One plate
806 of cells was removed, and the volume of the culture medium was measured. 37% formaldehyde
807 was added to achieve a final concentration of 1%, and the plates were incubated at 37°C for 10
808 minutes. Glycine (2.5 M) was then added to the plates at a final concentration of 125 mM to
809 terminate cross-linking. After mixing, the culture medium was left at room temperature for 5
810 minutes, and the cells were cleaned three times with cold PBS. The cells were scraped off with
811 PBS, centrifuged at 2,000g for 5 minutes, and the supernatant was removed. IP lysis solution
812 containing a protease inhibitor was added to lyse the cells (the amount of lysis solution
813 depending on the amount of cell precipitation), and the mixture was fully lysed on ice for 30
814 minutes, with the cells being repeatedly blown with a gun or shaken on a vortex mixer to ensure
815 complete lysis.

816 After sonication, the mixture was centrifuged at 12,000 rpm at 4°C for 10 minutes to remove
817 insoluble substances and collect the supernatant. 90 μL of the input was retained, and the rest
818 was stored at −80°C. To confirm the presence of the target protein in the sample, 40 μL of the
819 ultrasonic crushing product was taken, mixed with 10 μL of L5 reduced protein loading buffer, and
820 heated for denaturation before performing Western blot detection.

821 For the remaining 50 μL of the product, 5 μL of Protease K and 2 μL of 5M NaCl (final NaCl
822 concentration of 0.2M) were added and incubated at 55°C overnight for cross-linking. After
823 cross-linking, the nucleic acid concentration was measured, and a portion of the sample was
824 taken for PCR amplification, followed by agarose gel electrophoresis to detect the effectiveness of
825 ultrasonic fragmentation and confirm the presence of the target DNA. After verifying the Input
826 result, 100 μL of the ultrasonic crushing products was frozen at −80°C.

827 Next, 900 μL of ChIP Diffusion Buffer containing 1 mM PMSF and 20 μL of 50% of 1× PIC was
828 added, along with an additional 60 μL of Protein A+G Agarose/Salmon Sperm DNA. The mixture
829 was stirred at 4°C for 1 hour, allowed to stand at 4°C for 10 minutes to precipitate, and then
830 centrifuged at 4000 rpm for 5 minutes. The sample was divided into two 1.5 mL EP tubes; the
831 target protein IP antibody was added to one tube, while IgG (1 μg of the corresponding species)
832 was added to the other. The samples were shaken overnight at 4°C for precipitation and cleaning
833 of immune complexes.

834 After the overnight incubation, 200 μL of Protein A+G Agarose/Salmon Sperm DNA was
835 added to each tube, shaken at 4°C for 2 hours, allowed to stand at 4°C for 10 minutes, and then
836 centrifuged at 4,000 rpm for 1 minute. The supernatant was removed, and 8 μL of 5M NaCl and
837 20 μL of Protein K were added for overnight cross-linking at 55°C. Using databases like JASPAR to
838 predict transcription factor binding sites, primers were designed and synthesized based on these
839 binding sites. RT-PCR was employed to verify the binding, and after amplification, the products
840 were taken for gel electrophoresis to confirm the correct fragment size (Table S3).

841 Table S3

Gene name	Sequence
MMP9	5′-AGGCACTGAAGGAATGAGGC-3′
	5′-CCCCGCTTGGTGGAAAT-3′
RBMX2	5′-CTGACAGGAGGACCAGAGTTT-3′
	5′-TGCCTAGTTGTAGGGTTGAAGT-3′

842

843 Dual-luciferase reporter assay

844 293T cells in the logarithmic growth phase were adjusted to a density of 5×10^4 cells/mL and
845 inoculated into 48-well cell culture plates, with 300 cells per well. Each concentration gradient
846 was represented by three replicate wells. On the second day after plating, when the cells reached
847 a density of approximately 60-70%, transfection was performed with the following experimental
848 groups: pGL4.10 RRID:Addgene_72684 basic+pRL TK+Over NC, pGL4.10 basic+pRL TK+Over p65,
849 pGL4.10-*RBMX2*-WT+pRL TK+Over NC, pGL4.10-*RBMX2*-WT+pRL TK+Over p65,
850 pGL4.10-*RBMX2*-MUT+pRL TK+Over NC, pGL4.10-*RBMX2*-MUT+pRL TK+Over p65. Transfection
851 complexes were prepared, and dual-luciferase detection was carried out 48 hours
852 post-transfection.

853 For cell lysis, the cell culture medium was removed, and the cells were gently rinsed twice
854 with PBS. Then, 50 μL of 1× PLB lysis solution was added to each well, and the plates were placed
855 on a shaking table at room temperature for 15 minutes to ensure complete lysis.

856 From each sample, 20 μL was taken for measurement. To assess Firefly luciferase activity,
857 100 μL of Firefly luciferase detection reagent (LAR II reagent, Promega, USA) was added, mixed

858 well, and the relative light unit (RLU1) was measured. After this, 100 μL of Sea Kidney luciferase
859 detection reagent (1× Stop&Glo® Reagent, Promega, USA) was added, mixed thoroughly, and the
860 relative light unit (RLU2) was measured.

861 The activation level of the target reporter genes was compared between different samples
862 by calculating the ratio of RLU1 from the Firefly luciferase assay to RLU2 from the Sea Kidney
863 luciferase assay.

864

865 Protein docking

866 Molecular docking simulations were conducted to predict the formation of stable complexes
867 between proteins RBMX2 or MMP9 with p65. The aligned sequences of RBMX2, MMP9, and p65
868 proteins were sourced from the UniProt RRID:SCR_002380 database. Their three-dimensional
869 structures were predicted using AlphaFold and refined by constructing the structures in Avogadro.
870 The structures were then optimized using the MMFF94 force field and exported in PDB format for
871 further optimization in Gauss09.

872 The docking of the proteins was performed using Hdock, where each protein was treated
873 separately as the receptor and ligand to assess their interactions [79]. The resulting docking
874 affinities were annotated to provide insight into the binding interactions. Finally, PyMOL
875 RRID:SCR_000305 was utilized to visualize the binding interaction geometries, allowing for a
876 detailed examination of the molecular interactions between the proteins.

877

878 Statistical analysis

879 Statistical analysis was performed on all assays conducted in triplicate, with data expressed
880 as the mean ± standard error of the mean. Each experiment was independently repeated three
881 times. GraphPad Prism 7.0 RRID:SCR_002798 (La Jolla) was utilized for statistical analysis,
882 employing a two-tailed unpaired t-test with Welch's correction for comparisons between two
883 groups. For comparisons among multiple groups, one-way or two-way ANOVA was applied,
884 followed by the LSD test. Statistical significance was indicated at four levels: not significant (ns
885 presents $p > 0.05$), * presents $p < 0.05$, ** presents $p < 0.01$, and *** presents $p < 0.001$.

886 **Acknowledgments**

887 We would like to thank the National Key Laboratory of Agricultural Microbiology Core
888 Facility for assistance in high-throughput microscopy, and we are grateful to Zhe Hu for his
889 support of the sample preparation. This work was supported by the Major projects of agricultural
890 biological breeding in China (2023ZD0405003), the National Natural Science Foundation of China
891 (32072942), China Agriculture Research System of MOF and MARA (CARS-37), National Natural
892 Science Foundation of China (81960772) and Key Project of Inner Mongolia Medical University
893 (YKD2022ZD016).

894 **Author Contributions**

895 YC and AG contributed to the conception and design of the study. CW, YP and HY carried out
896 the experiment and wrote sections of the manuscript and made equal contribution. YJ, AK, ZY, KZ,
897 and SX were involved in bacterial and cell research studies. CW, PY, HY, SX, LB, LZ, and CH
898 performed the statistical analysis. CW, AG, and YC wrote the manuscript with all authors
899 providing feedback. All authors contributed to manuscript revision, proof-reading, and approval
900 of the submitted version.

901 **Conflict of Interest**

902 The authors declare that the research was conducted in the absence of any commercial or
903 financial relationships that could be construed as a potential conflict of interest.

904

905

906

907 **References**

908 1. WHO, Global tuberculosis report. 2023.
909 2. Preda, M.; Tănase, B. C.; Zob, D. L.; Gheorghe, A. S.; Lungulescu, C. V.;
910 Dumitrescu, E. A.; Stănculeanu, D. L.; Manolescu, L. S. C.; Popescu, O.; Ibraim, E.; Mahler,
911 B., The Bidirectional Relationship between Pulmonary Tuberculosis and Lung Cancer. Int J Environ
912 Res Public Health 2023, 20 (2).
913 3. Cabrera-Sanchez, J.; Cuba, V.; Vega, V.; Van der Stuyft, P.; Otero, L., Lung cancer
914 occurrence after an episode of tuberculosis: a systematic review and meta-analysis. Eur Respir
915 Rev 2022, 31 (165).
916 4. Suarez-Carmona, M.; Lesage, J.; Cataldo, D.; Gilles, C., EMT and inflammation:
917 inseparable actors of cancer progression. Mol Oncol 2017, 11 (7), 805-823.
918 5. Wang, C.; Jiang, Y.; Yang, Z.; Xu, H.; Khalid, A. K.; Iftakhar, T.; Peng, Y.; Lu, L.;
919 Zhang, L.; Bermudez, L.; Guo, A.; Chen, Y., Host factor RBMX2 promotes epithelial cell

920 apoptosis by downregulating APAF-1's Retention Intron after Mycobacterium bovis infection.
921 Front Immunol 2024, 15, 1431207.
922 6. Song, Y.; He, S.; Ma, X.; Zhang, M.; Zhuang, J.; Wang, G.; Ye, Y.; Xia, W.,
923 RBMX contributes to hepatocellular carcinoma progression and sorafenib resistance by
924 specifically binding and stabilizing BLACAT1. Am J Cancer Res 2020, 10 (11), 3644-3665.
925 7. Schümann, F. L.; Bauer, M.; Groß, E.; Terziev, D.; Wienke, A.; Wickenhauser, C.;
926 Binder, M.; Weber, T., RBMX Protein Expression in T-Cell Lymphomas Predicts Chemotherapy
927 Response and Prognosis. Cancers (Basel) 2021, 13 (19).
928 8. Alors-Pérez, E.; Blázquez-Encinas, R.; Moreno-Montilla, M. T.; García-Vioque, V.;
929 Jiménez-Vacas, J. M.; Mafficini, A.; González-Borja, I.; Luchini, C.; Sánchez-Hidalgo, J. M.;
930 Sánchez-Frías, M. E.; Pedraza-Arevalo, S.; Romero-Ruiz, A.; Lawlor, R. T.; Viúdez, A.;
931 Gahete, M. D.; Scarpa, A.; Arjona-Sánchez, Á.; Luque, R. M.; Ibáñez-Costa, A.; Castaño, J.
932 P., Spliceosomic dysregulation in pancreatic cancer uncovers splicing factors PRPF8 and RBMX as
933 novel candidate actionable targets. Mol Oncol 2024, 18 (10), 2524-2540.
934 9. Wibbe, N.; Ebnet, K., Cell Adhesion at the Tight Junctions: New Aspects and New
935 Functions. Cells-Basel 2023, 12 (23).
936 10. Bhat, A. A.; Uppada, S.; Achkar, I. W.; Hashem, S.; Yadav, S. K.; Shanmugakonar,
937 M.; Al-Naemi, H. A.; Haris, M.; Uddin, S., Tight Junction Proteins and Signaling Pathways in
938 Cancer and Inflammation: A Functional Crosstalk. Front Physiol 2018, 9, 1942.
939 11. Zou, Y.; Xiang, Q.; Wang, J.; Peng, J.; Wei, H., Oregano Essential Oil Improves
940 Intestinal Morphology and Expression of Tight Junction Proteins Associated with Modulation of
941 Selected Intestinal Bacteria and Immune Status in a Pig Model. Biomed Res Int 2016, 2016,
942 5436738.
943 12. Edelblum, K. L.; Turner, J. R., The tight junction in inflammatory disease: communication
944 breakdown. Curr Opin Pharmacol 2009, 9 (6), 715-20.
945 13. Bell, C. E.; Watson, A. J., p38 MAPK regulates cavitation and tight junction function in
946 the mouse blastocyst. Plos One 2013, 8 (4), e59528.
947 14. Kitagawa, N.; Inai, Y.; Higuchi, Y.; Iida, H.; Inai, T., Inhibition of JNK in HaCaT cells
948 induced tight junction formation with decreased expression of cytokeratin 5, cytokeratin 17 and
949 desmoglein 3. Histochem Cell Biol 2014, 142 (4), 389-99.
950 15. Lin, X.; Zhu, Y.; Le, G., Tetramethylpyrazine Alleviates Tight Junction Disruption of
951 Bronchial Mucosal Epithelial Cells Caused by Interleukin-17 via Inhibiting Nuclear
952 Factor-κB-p65/Tumor Necrosis Factor-α Signaling Pathway. J Interferon Cytokine Res 2021, 41
953 (11), 415-424.
954 16. Jeong, C. H.; Seok, J. S.; Petriello, M. C.; Han, S. G., Arsenic downregulates tight
955 junction claudin proteins through p38 and NF-κB in intestinal epithelial cell line, HT-29. Toxicology
956 2017, 379, 31-39.
957 17. Singh, V.; Phukan, U. J., Interaction of host and Staphylococcus aureus protease-system
958 regulates virulence and pathogenicity. Med Microbiol Immunol 2019, 208 (5), 585-607.
959 18. Gu, L.; Wang, H.; Guo, Y. L.; Zen, K., Heparin blocks the adhesion of E. coli O157:H7
960 to human colonic epithelial cells. Biochem Biophys Res Commun 2008, 369 (4), 1061-4.
961 19. Harrandah, A. M.; Chukkapalli, S. S.; Bhattacharyya, I.; Progulske-Fox, A.; Chan, E.
962 K. L., Fusobacteria modulate oral carcinogenesis and promote cancer progression. J Oral
963 Microbiol 2021, 13 (1).

964 20. Li, N. S.; Xu, X. B.; Yang, H.; Wang, H.; Ouyang, Y. B.; Zhou, Y. A.; Peng, C.;
965 Yuan, Z. X.; He, C.; Zeng, C. Y.; Hong, J. B., Activation of Aquaporin 5 by carcinogenic infection
966 promotes epithelial-mesenchymal transition via the MEK/ERK pathway. Helicobacter 2021, 26 (5).
967 21. Bessède, E.; Dubus, P.; Mégraud, F.; Varon, C., infection and stem cells at the origin
968 of gastric cancer. Oncogene 2015, 34 (20), 2547-2555.
969 22. Ferluga, J.; Yasmin, H.; Al-Ahdal, M. N.; Bhakta, S.; Kishore, U., Natural and trained
970 innate immunity against. Immunobiology 2020, 225 (3).
971 23. Strong, E. J.; Wang, J.; Ng, T. W.; Porcelli, S. A.; Lee, S., Mycobacterium
972 tuberculosis PPE51 Inhibits Autophagy by Suppressing Toll-Like Receptor 2-Dependent Signaling.
973 Mbio 2022, 13 (3).
974 24. Vignesh, R.; Balakrishnan, P.; Tan, H. Y.; Yong, Y. K.; Velu, V.; Larsson, M.;
975 Shankar, E. M., Tuberculosis-Associated Immune Reconstitution Inflammatory Syndrome-An
976 Extempore Game of Misfiring with Defense Arsenals. Pathogens 2023, 12 (2).
977 25. Certo, M.; Tsai, C. H.; Pucino, V.; Ho, P. C.; Mauro, C., Lactate modulation of
978 immune responses in inflammatory versus tumour microenvironments. Nat Rev Immunol 2021,
979 21 (3), 151-161.
980 26. Harmon, C.; O'Farrelly, C.; Robinson, M. W., The Immune Consequences of Lactate in
981 the Tumor Microenvironment. Tumor Microenvironment: Molecular Players, Pt A 2020, 1259,
982 113-124.
983 27. Rodel, H. E.; Ferreira, I. A. T. M.; Ziegler, C. G. K.; Ganga, Y.; Bernstein, M.; Hwa,
984 S. H.; Nargan, K.; Lustig, G.; Kaplan, G.; Noursadeghi, M.; Shalek, A. K.; Steyn, A. J. C.;
985 Sigal, A., Aggregated Enhances the Inflammatory Response. Front Microbiol 2021, 12.
986 28. Park, D. W.; Moon, S. M.; Choi, H.; Kim, S. H.; Kang, H. K.; Jung, J. H.; Han, K.;
987 Shin, D. W.; Lee, H., Increased lung cancer risk and associated risk factors in tuberculosis survivors:
988 a Korean population-based study. Cancer Res 2023, 83 (7).
989 29. Hu, M., A Case of Multi-Organ Tuberculosis Misdiagnosed as Lung Cancer and a
990 Literature Review. Cancer Manag Res 2023, 15, 1395-1400.
991 30. Menakuru, S.; Dhillon, V.; Emran, J.; Khan, I.; Beirat, A.; Salih, A., Are Delays In
992 The Diagnosis Of Lung Cancer Due To Patients First Seeking Treatment for Tuberculosis In Rural
993 India? J Thorac Oncol 2023, 18 (3), E23-E23.
994 31. Liu, W.; Wang, H.; Bai, F.; Ding, L.; Huang, Y.; Lu, C.; Chen, S.; Li, C.; Yue,
995 X.; Liang, X.; Ma, C.; Xu, L.; Gao, L., IL-6 promotes metastasis of non-small-cell lung cancer
996 by up-regulating TIM-4 via NF-κB. Cell Prolif 2020, 53 (3), e12776.
997 32. Shrestha, R.; Bridle, K. R.; Crawford, D. H. G.; Jayachandran, A., TNF-α-mediated
998 epithelial-to-mesenchymal transition regulates expression of immune checkpoint molecules in
999 hepatocellular carcinoma. Mol Med Rep 2020, 21 (4), 1849-1860.
1000 33. Hao, Y.; Baker, D.; Ten Dijke, P., TGF-β-Mediated Epithelial-Mesenchymal Transition
1001 and Cancer Metastasis. Int J Mol Sci 2019, 20 (11).
1002 34. Xu, G.; Li, Y.; Yang, J.; Zhou, X.; Yin, X.; Liu, M.; Zhao, D., Effect of recombinant
1003 Mce4A protein of Mycobacterium bovis on expression of TNF-alpha, iNOS, IL-6, and IL-12 in
1004 bovine alveolar macrophages. Mol Cell Biochem 2007, 302 (1-2), 1-7.
1005 35. Na, T. Y.; Schecterson, L.; Mendonsa, A. M.; Gumbiner, B. M., The functional activity
1006 of E-cadherin controls tumor cell metastasis at multiple steps. P Natl Acad Sci USA 2020, 117 (11),
1007 5931-5937.

1008 36. Fedele, M.; Sgarra, R.; Battista, S.; Cerchia, L.; Manfioletti, G., The
1009 Epithelial-Mesenchymal Transition at the Crossroads between Metabolism and Tumor
1010 Progression. Int J Mol Sci 2022, 23 (2).
1011 37. Alqurashi, Y. E.; Al-Hetty, H. R. A. K.; Ramaiah, P.; Fazaa, A. H.; Jalil, A. T.;
1012 Alsaikhan, F.; Gupta, J.; Ramírez-Coronel, A. A.; Tayyib, N. A.; Peng, H., Harnessing function
1013 of EMT in hepatocellular carcinoma: From biological view to nanotechnological standpoint.
1014 Environ Res 2023, 227.
1015 38. Mirzaei, S.; Saghari, S.; Bassiri, F.; Raesi, R.; Zarrabi, A.; Hushmandi, K.; Sethi,
1016 G.; Tergaonkar, V., NF-κB as a regulator of cancer metastasis and therapy response: A focus on
1017 epithelial-mesenchymal transition. J Cell Physiol 2022, 237 (7), 2770-2795.
1018 39. O'Leary, K.; Shia, A.; Schmid, P., Epigenetic Regulation of EMT in Non-Small Cell Lung
1019 Cancer. Curr Cancer Drug Tar 2018, 18 (1), 89-96.
1020 40. Stefani, C.; Miricescu, D.; Stanescu-Spinu, I. I.; Nica, R. I.; Greabu, M.; Totan, A.
1021 R.; Jinga, M., Growth Factors, PI3K/AKT/mTOR and MAPK Signaling Pathways in Colorectal Cancer
1022 Pathogenesis: Where Are We Now? Int J Mol Sci 2021, 22 (19).
1023 41. Kim, B. K.; Kim, D. M.; Park, H.; Kim, S. K.; Hwang, M. A.; Lee, J.; Kang, M. J.;
1024 Byun, J. E.; Im, J. Y.; Kang, M.; Park, K. C.; Yeom, Y. I.; Kim, S. Y.; Jung, H.; Kweon, D. H.;
1025 Cheong, J. H.; Won, M., Synaptotagmin 11 scaffolds MKK7-JNK signaling process to promote
1026 stem-like molecular subtype gastric cancer oncogenesis. J Exp Clin Canc Res 2022, 41 (1).
1027 42. Gonzalez-Avila, G.; Sommer, B.; García-Hernández, A. A.; Ramos, C., Matrix
1028 Metalloproteinases' Role in Tumor Microenvironment. Tumor Microenvironment: Extracellular
1029 Matrix Components - Pt A 2020, 1245, 97-131.
1030 43. Cox, T. R., The matrix in cancer. Nat Rev Cancer 2021, 21 (4), 217-238.
1031 44. Kwaan, H. C.; Lindholm, P. F., Fibrin and Fibrinolysis in Cancer. Semin Thromb Hemost
1032 2019, 45 (4), 413-422.
1033 45. Mego, M.; Karaba, M.; Minarik, G.; Benca, J.; Sedlácková, T.; Tothova, L.;
1034 Vlkova, B.; Cierna, Z.; Janega, P.; Luha, J.; Gronesova, P.; Pindak, D.; Fridrichova, I.;
1035 Celec, P.; Reuben, J. M.; Cristofanilli, M.; Mardiak, J., Relationship between Circulating Tumor
1036 Cells, Blood Coagulation, and Urokinase-Plasminogen-Activator System in Early Breast Cancer
1037 Patients. Breast J 2015, 21 (2), 155-160.
1038 46. Kim, J. H., Interleukin-8 in the Tumor Immune Niche: Lessons from Comparative
1039 Oncology. Tumor Microenvironment: The Role of Interleukins, Pt A 2020, 1240, 25-33.
1040 47. Zuo, J. H.; Zhu, W.; Li, M. Y.; Li, X. H.; Yi, H.; Zeng, G. Q.; Wan, X. X.; He, Q.
1041 Y.; Li, J. H.; Qu, J. Q.; Chen, Y.; Xiao, Z. Q., Activation of EGFR promotes squamous carcinoma
1042 SCC10A cell migration and invasion via inducing EMT-like phenotype change and
1043 MMP-9-mediated degradation of E-cadherin. J Cell Biochem 2011, 112 (9), 2508-17.
1044 48. Peng, W.; Jiang, J.; Fu, J.; Duan, H.; Wang, J.; Duan, C., lncRNA GMDS-AS1
1045 restrains lung adenocarcinoma progression via recruiting TAF15 protein to stabilize SIRT1 mRNA.
1046 Epigenomics 2023, 15 (7), 417-434.
1047 49. Reis, A. C.; Cunha, M. V., The open pan- genome architecture and virulence landscape
1048 of Mycobacterium bovis. Microb Genomics 2021, 7 (10).
1049 50. Fan, Y. L.; Wu, J. B.; Cheng, X. W.; Zhang, F. Z.; Feng, L. S., Fluoroquinolone
1050 derivatives and their anti-tubercular activities. Eur J Med Chem 2018, 146, 554-563.
1051 51. Borkowska, D. I.; Napiórkowska, A. M.; Brzezinska, S. A.; Kozinska, M.; Zabost, A.

1052 T.; Augustynowicz-Kopec, E. M., From Latent Tuberculosis Infection to Tuberculosis. News in
1053 Diagnostics (QuantiFERON-Plus). Pol J Microbiol 2017, 66 (1), 5-8.
1054 52. Rastogi, N.; Zarin, S.; Alam, A.; Konduru, G. V.; Manjunath, P.; Mishra, A.;
1055 Kumar, S.; Nagarajaram, H. A.; Hasnain, S. E.; Ehtesham, N. Z., Structural and Biophysical
1056 properties of therapeutically important proteins Rv1509 and Rv2231A of Mycobacterium
1057 tuberculosis. Int J Biol Macromol 2023, 245.
1058 53. Corleis, B.; Dorhoi, A., Early dynamics of innate immunity during pulmonary
1059 tuberculosis. Immunol Lett 2020, 221, 56-60.
1060 54. Abebe, F., Crosstalk between Mycobacterium tuberculosis and the host cell. Clin Exp
1061 Immunol 2021, 204 (1), 32-40.
1062 55. Reuschl, A. K.; Edwards, M. R.; Parker, R.; Connell, D. W.; Hoang, L.; Halliday, A.;
1063 Jarvis, H.; Siddiqui, N.; Wright, C.; Bremang, S.; Newton, S. M.; Beverley, P.; Shattock, R.
1064 J.; Kon, M.; Lalvanl, A., Innate activation of human primary epithelial cells broadens the host
1065 response to in the airways. Plos Pathog 2017, 13 (9).
1066 56. Dorhoi, A.; Kaufmann, S. H. E., Perspectives on host adaptation in response to:
1067 Modulation of inflammation. Semin Immunol 2014, 26 (6), 533-542.
1068 57. Rajararna, M. V. S.; Ni, B.; Dodd, C. E.; Schlesinger, L. S., Macrophage
1069 immunoregulatory pathways in tuberculosis. Semin Immunol 2014, 26 (6), 471-485.
1070 58. D'Agnillo, F.; Walters, K. A.; Xiao, Y. L.; Sheng, Z. M.; Scherler, K.; Park, J.;
1071 Gygli, S.; Rosas, L. A.; Sadtler, K.; Kalish, H.; Blatti, C. A.; Zhu, R. Q.; Gatzke, L.;
1072 Bushell, C.; Memoli, M. J.; O'Day, S. J.; Fischer, T. D.; Hammond, T. C.; Lee, R. C.; Cash, J.
1073 C.; Powers, M. E.; O'Keefe, G. E.; Butnor, K. J.; Rapkiewicz, A. V.; Travis, W. D.; Layne, S.
1074 P.; Kash, J. C.; Taubenberger, J. K., Lung epithelial and endothelial damage, loss of tissue repair,
1075 inhibition of fibrinolysis, and cellular senescence in fatal COVID-19. Sci Transl Med 2021, 13 (620).
1076 59. Barros, B. C. S. C.; Almeida, B. R.; Barros, D. T. L.; Toledo, M. S.; Suzuki, E.,
1077 Respiratory Epithelial Cells: More Than Just a Physical Barrier to Fungal Infections. J Fungi 2022, 8
1078 (6).
1079 60. Hu, Y.; Mu, H. S.; Deng, Z. P., RBM14 as a novel epigenetic-activated tumor oncogene
1080 is implicated in the reprogramming of glycolysis in lung cancer. World J Surg Oncol 2023, 21 (1).
1081 61. Buckley, A.; Turner, J. R., Cell Biology of Tight Junction Barrier Regulation and Mucosal
1082 Disease. Csh Perspect Biol 2018, 10 (1).
1083 62. Rastegar, D. A.; Tabar, M. S.; Alikhani, M.; Parsamatin, P.; Samani, F. S.;
1084 Sabbaghian, M.; Gilani, M. A. S.; Ahadi, A. M.; Meybodi, A. M.; Piryaei, A.; Ansari-Pour,
1085 N.; Gourabi, H.; Baharvand, H.; Salekdeh, G. H., Isoform-Level Gene Expression Profiles of
1086 Human Y Chromosome Azoospermia Factor Genes and Their X Chromosome Paralogs in the
1087 Testicular Tissue of Non-Obstructive Azoospermia Patients. J Proteome Res 2015, 14 (9),
1088 3595-3605.
1089 63. Zhu, Y. C.; Zheng, M. H.; Song, D. L.; Ye, L.; Wang, X. D., Global comparison of
1090 chromosome X genes of pulmonary telocytes with mesenchymal stem cells, fibroblasts, alveolar
1091 type II cells, airway epithelial cells, and lymphocytes. J Transl Med 2015, 13.
1092 64. Zhang, X. T.; Zhang, J. R.; Zhao, W.; Dong, X.; Xin, P.; Liu, X.; Li, X. J.; Jing, Z.
1093 F.; Zhang, Z.; Kong, C. Z.; Yu, X. Y., Long non-coding RNA LINC02446 suppresses the
1094 proliferation and metastasis of bladder cancer cells by binding with EIF3G and regulating the
1095 mTOR signalling pathway. Cancer Gene Ther 2021, 28 (12), 1376-1389.

1096 65. Savagner, P., Epithelial-Mesenchymal Transitions: From Cell Plasticity to Concept
1097 Elasticity. Curr Top Dev Biol 2015, 112, 273-300.
1098 66. Kyuno, D.; Takasawa, A.; Kikuchi, S.; Takemasa, I.; Osanai, M.; Kojima, T., Role of
1099 tight junctions in the epithelial-to-mesenchymal transition of cancer cells. Bba-Biomembranes
1100 2021, 1863 (3).
1101 67. Hashimoto, I.; Oshima, T., Claudins and Gastric Cancer: An Overview. Cancers 2022, 14
1102 (2).
1103 68. Malfertheiner, P.; Camargo, M. C.; El-Omar, E.; Liou, J. M.; Peek, R.; Schulz, C.;
1104 Smith, S. I.; Suerbaum, S., Helicobacter pylori infection. Nat Rev Dis Primers 2023, 9 (1).
1105 69. de Brito, B. B.; da Silva, F. A. F.; Soares, A. S.; Pereira, V. A.; Santos, M. L. C.;
1106 Sampaio, M. M.; Neves, P. H. M.; de Melo, F. F., Pathogenesis and clinical management of
1107 gastric infection. World J Gastroentero 2019, 25 (37), 5578-5589.
1108 70. Ho, J. C. M.; Leung, C. C., Management of co-existent tuberculosis and lung cancer. Lung
1109 Cancer 2018, 122, 83-87.
1110 71. Christopoulos, A.; Saif, M. W.; Sarris, E. G.; Syrigos, K. N., Epidemiology of active
1111 tuberculosis in lung cancer patients: a systematic review. Clin Respir J 2014, 8 (4), 375-381.
1112 72. Nalbandian, A.; Yan, B. S.; Pichugin, A.; Bronson, R. T.; Kramnik, I., Lung
1113 carcinogenesis induced by chronic tuberculosis infection: the experimental model and genetic
1114 control. Oncogene 2009, 28 (17), 1928-1938.
1115 73. Holla, S.; Ghorpade, D. S.; Singh, V.; Bansal, K.; Balaji, K. N., BCG promotes tumor
1116 cell survival from tumor necrosis factor-α-induced apoptosis. Mol Cancer 2014, 13.
1117 74. Gupta, P. K.; Tripathi, D.; Kulkarni, S.; Rajan, M. G. R., H37Rv infected THP-1 cells
1118 induce epithelial mesenchymal transition (EMT) in lung adenocarcinoma epithelial cell line (A549).
1119 Cell Immunol 2016, 300, 33-40.
1120 75. Leung, C. Y.; Huang, H. L.; Rahman, M. M.; Nomura, S.; Abe, S. K.; Saito, E.;
1121 Shibuya, K., Cancer incidence attributable to tuberculosis in 2015: global, regional, and national
1122 estimates. Bmc Cancer 2020, 20 (1).
1123 76. De La Barrera, S.; Alemán, M.; Musella, R.; Schierloh, P.; Pasquinelli, V.; García,
1124 V.; Abbate, E.; Sasiain, M. D., IL-10 down-regulates costimulatory molecules on-pulsed
1125 macrophages and impairs the lytic activity of CD4 and CD8 CTL in tuberculosis patients. Clin Exp
1126 Immunol 2004, 138 (1), 128-138.
1127 77. Chen, X.; Huang, J.; Zhu, H. M.; Guo, Y. P.; Khan, F. A.; Menghwar, H.; Zhao,
1128 G.; Guo, A. Z., P27 (MBOV_RS03440) is a novel fibronectin binding adhesin of Mycoplasma bovis.
1129 Int J Med Microbiol 2018, 308 (7), 848-857.
1130 78. Zhao, G.; Zhu, X. F.; Zhang, H.; Chen, Y. Y.; Schieck, E.; Hu, C. M.; Chen, H. C.;
1131 Guo, A., Novel Secreted Protein of MbovP280 Induces Macrophage Apoptosis Through CRYAB.
1132 Front Immunol 2021, 12.
1133 79. Li, T.; He, J.; Cao, H.; Zhang, Y.; Chen, J.; Xiao, Y.; Huang, S. Y., All-atom RNA
1134 structure determination from cryo-EM maps. Nat Biotechnol 2024.

1135

1136

1137

FIG1

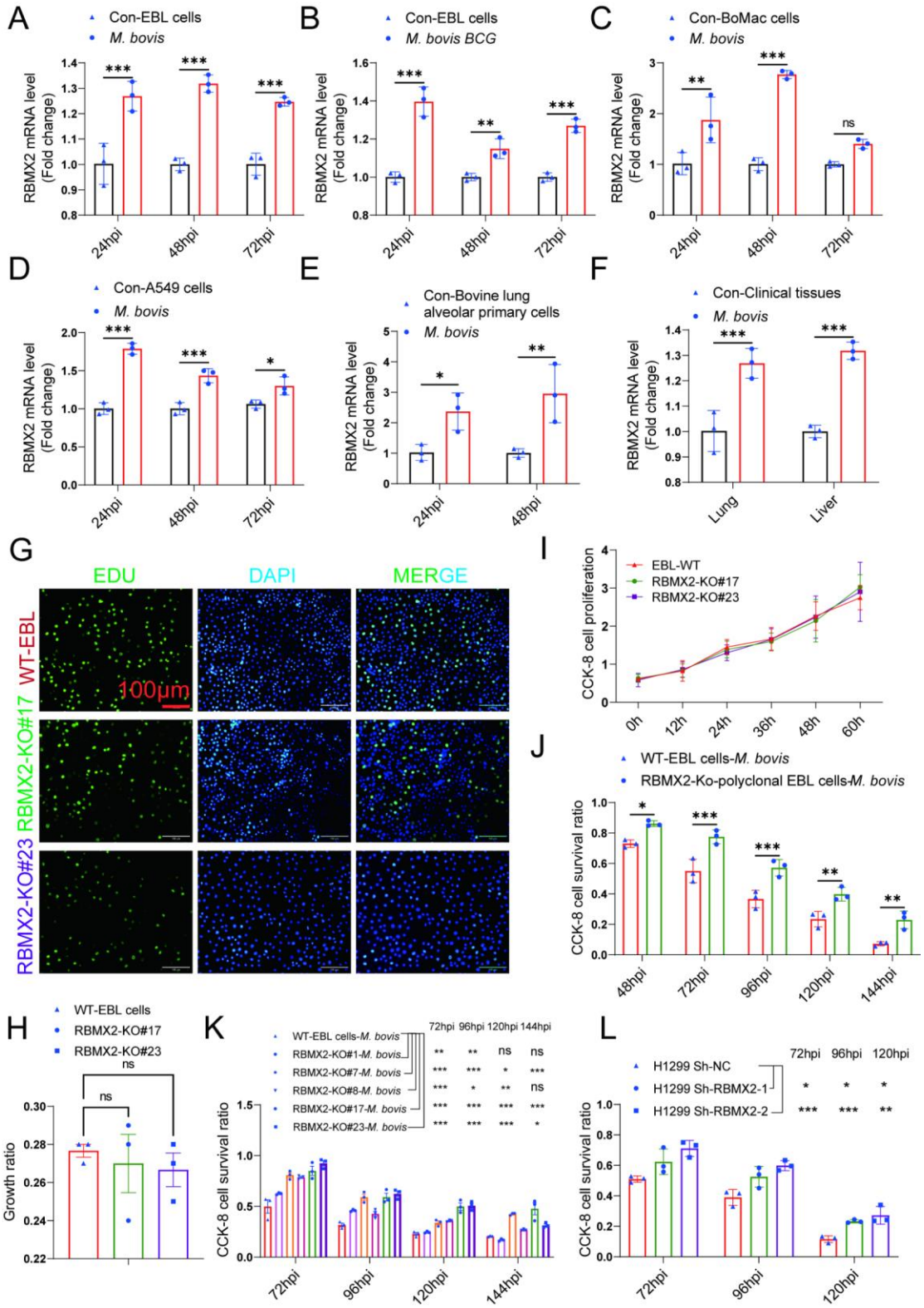
A
Con-EBL cells
M. bovis
RBMX2 mRNA level (Fold change)
24hpi
48hpi
72hpi
B
Con-EBL cells
M. bovis BCG
C
Con-BoMac cells
M. bovis
ns
D
Con-A549 cells
M. bovis
E
Con-Bovine lung alveolar primary cells
M. bovis
F
Con-Clinical tissues
M. bovis
Lung
Liver
G
EDU
DAPI
MERGE
WT-EBL
RBMX2-KO#17
RBMX2-KO#23
100μm
I
EBL-WT
RBMX2-KO#17
RBMX2-KO#23
CCK-8 cell proliferation
0h
12h
24h
36h
48h
60h
J
WT-EBL cells-M. bovis
RBMX2-Ko-polyclonal EBL cells-M. bovis
CCK-8 cell survival ratio
48hpi
72hpi
96hpi
120hpi
144hpi
H
WT-EBL cells
RBMX2-KO#17
RBMX2-KO#23
Growth ratio
K
WT-EBL cells-M. bovis
RBMX2-KO#1-M. bovis
RBMX2-KO#7-M. bovis
RBMX2-KO#8-M. bovis
RBMX2-KO#17-M. bovis
RBMX2-KO#23-M. bovis
L
H1299 Sh-NC
H1299 Sh-RBMX2-1
H1299 Sh-RBMX2-2

1143

1144

1145 **FIGURE 1| Expression of *RBMX2* after infection, and *RBMX2* did not affect cell proliferation but**
1146 **inhibited cell survival during *M. bovis* infection.**
1147 (A, B) The expression of *RBMX2* in EBL cells infected by (A) *M. bovis* and (B) *M. bovis* BCG were
1148 analyzed by RT-qPCR. Data were represented by fold expression relative to uninfected cells.
1149 (C,-E) The expression of *RBMX2* mRNA in (E) BoMac cells, (F) A549 cells, and (G) bovine lung
1150 alveolar primary cells infected by *M. bovis* were analyzed via RT-qPCR. Data were represented by
1151 fold expression relative to uninfected cells.
1152 (F) The expression of *RBMX2* mRNA in clinical TB tissues infected by *M. bovis* via RT-qPCR. Data
1153 were represented by fold expression relative to uninfected tissues.
1154 (G, H) The effect of *RBMX2* on the proliferation of EBL cells was observed by EDU assay. Data
1155 were represented by the Fluorescence cells relative to WT EBL cells.
1156 (I) The effect of *RBMX2* on the proliferation of EBL cells was observed by CCK-8 assay. Data were
1157 represented by the absorbance value relative to WT EBL cells.
1158 (J) Detection of the ability of *RBMX2* knockout Polyclonal EBL cells resisting to *M. bovis* infection
1159 by CCK-8 assay. Data were represented by the absorbance value relative to WT EBL cells after *M.*
1160 *bovis* infection.
1161 (K) Detection of the ability of different *RBMX2* knockout site Monoclonal EBL cells against *M.*
1162 *bovis* infection by CCK-8 assay. Data were represented by the absorbance value relative to WT
1163 EBL cells after *M. bovis* infection.
1164 (L) Detection of the ability of *RBMX2* slicing H1299 cells against *M. bovis* infection by CCK-8 assay.
1165 Data were represented by the absorbance value relative to Sh-NC H1299 cells after *M. bovis*
1166 infection.
1167 One-way ANOVA and two-way ANOVA were used to determine the statistical significance of
1168 differences between different groups. Ns presents no significance, * presents $p < 0.05$,
1169 **presents $p < 0.01$, and *** presents $p < 0.001$ indicate statistically significant differences. Data
1170 were representative of at least three independent experiments.

1171

1172

1173

1174

1175

1176

1177

1178

1179

1180

FIG2

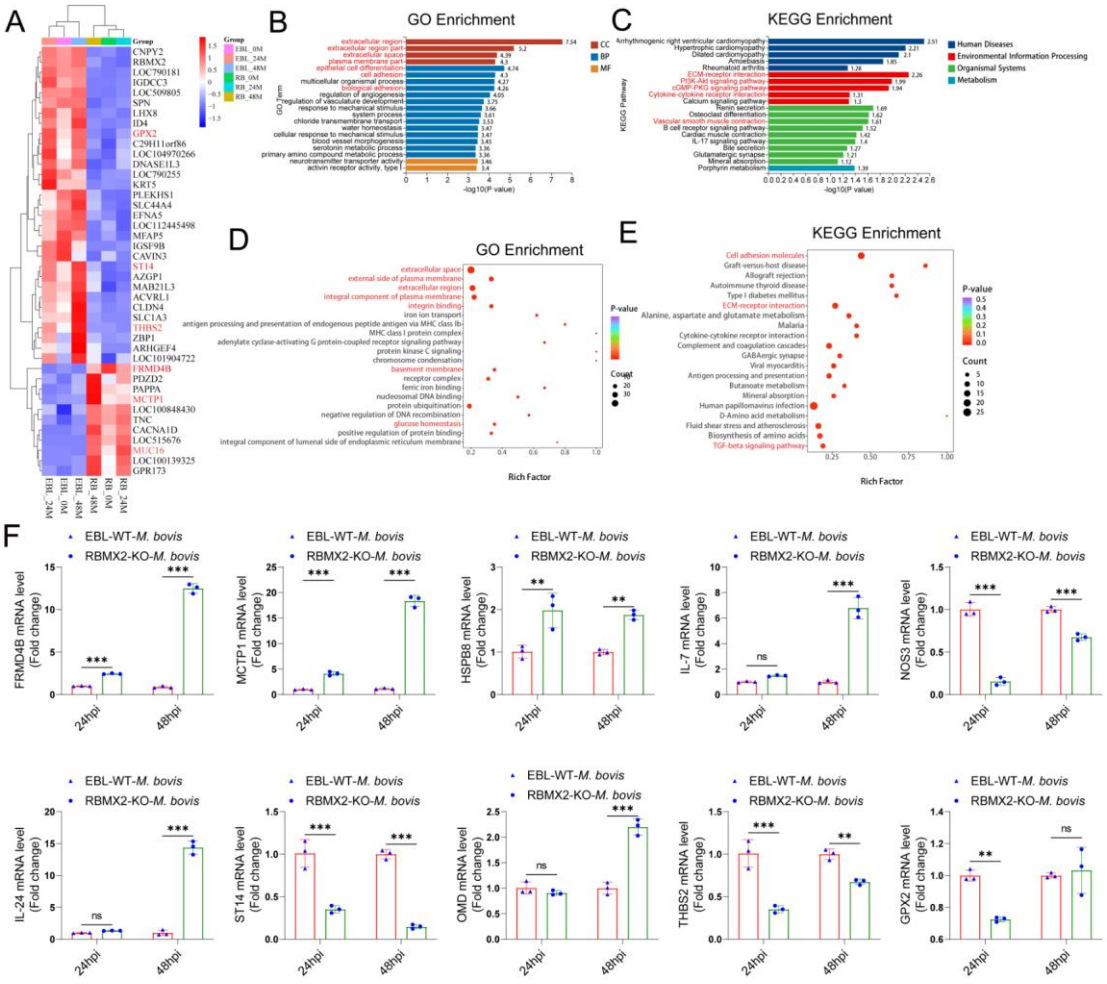
A
B
GO Enrichment
C
KEGG Enrichment
D
GO Enrichment
E
KEGG Enrichment
F
EBL-WT-M. bovis
RBMX2-KO-M. bovis
FRMD4B mRNA level (Fold change)
MCTP1 mRNA level (Fold change)
HSPB8 mRNA level (Fold change)
IL-7 mRNA level (Fold change)
NOS3 mRNA level (Fold change)
IL-24 mRNA level (Fold change)
ST14 mRNA level (Fold change)
OMD mRNA level (Fold change)
THBS2 mRNA level (Fold change)
GPX2 mRNA level (Fold change)
24hpi
48hpi

1200

1201 **FIGURE 2| Transcriptome and proteomic analysis in *RBMX2* knockout and WT EBL cells after *M.***
1202 ***bovis* infection.**

1203 (A) The heat map illustrates some genes that had been all enriched in RBMX2 knockout and WT
1204 EBL cells after *M. bovis* infection in 0, 24, and 48hpi. Red represents upregulated genes, and blue
1205 represents downregulated genes. Each group represented three independent samples.

1206 (B) GO Analysis of all enriched genes in 0, 24 and 48hpi. Data were represented as all enriched
1207 pathways in RBMX2 knockout EBL cells relative to WT EBL cells after *M. bovis* infection thrice.

1208 (C) KEGG Analysis of all enriched genes in 0, 24, and 48hpi. Data were represented as all enriched
1209 pathways in RBMX2 knockout EBL cells relative to WT EBL cells after *M. bovis* infection in three
1210 times.

1211 (D) GO Analysis of all enriched proteins in 48hpi. Data were represented as all enriched pathways
1212 in RBMX2 knockout EBL cells relative to WT EBL cells after *M. bovis* infection.

1213 (E) KEGG Analysis of all enriched genes in 48hpi. Data were represented as all enriched pathways
1214 in RBMX2 knockout EBL cells relative to WT EBL cells after *M. bovis*-infection (MOI 20) in three
1215 times.

1216 (F) Identification the expression of related genes mRNA enriched by RT-qPCR. Data were
1217 represented as the fold expression in RBMX2 knockout EBL cells relative to WT EBL cells after *M.*
1218 *bovis* infection.

1219 Two-way ANOVA was used to determine the statistical significance of differences between
1220 different groups. Ns presents no significance, * presents $p < 0.05$, **presents $p < 0.01$, and ***
1221 presents $p < 0.001$ indicate statistically significant differences.

1222

1223

1224

1225

1226

1227

1228

1229

1230

1231

1232

1233

1234

1235

FIG3

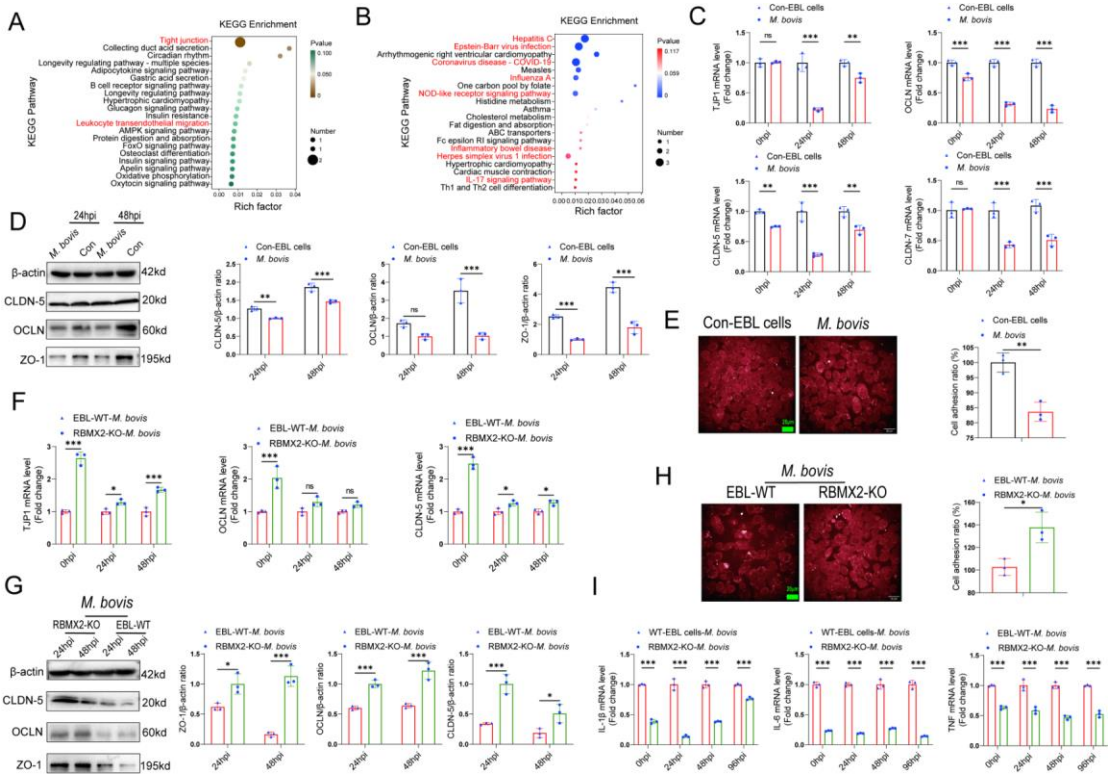
A
KEGG Enrichment
KEGG Pathway
Rich factor
B
KEGG Enrichment
KEGG Pathway
Rich factor
C
Con-EBL cells
M. bovis
D
24hpi
48hpi
M. bovis
Con
β-actin
CLDN-5
OCLN
ZO-1
42kd
20kd
60kd
195kd
E
Con-EBL cells
M. bovis
Cell adhesion ratio (%)
F
EBL-WT-M. bovis
RBMX2-KO-M. bovis
G
M. bovis
RBMX2-KO
EBL-WT
H
M. bovis
EBL-WT
RBMX2-KO
I
WT-EBL cells-M. bovis
RBMX2-KO-M. bovis

1261
1262 **FIGURE 3| *RBMX2* had the potential to induce the disruption of tight junctions in EBL cells after**
1263 ***M. bovis* infection.**
1264 (A, B) KEGG analysis was conducted to identify the (A) down-regulated and (B) up-regulated
1265 pathways among the enriched genes after *M. bovis* infection of WT EBL cells. Data were relative
1266 to WT EBL cells without *M. bovis* infection.
1267 (C, D) The expression of epithelial cells tight junction-related (C) mRNAs (*TJP1*, *CLDN-5*, *CLDN-7,*
1268 and *OCLN*) and (D) proteins (ZO-1, CLDN-5, and OCLN) were assessed after *M. bovis* infection of
1269 WT EBL cells via RT-qPCR and WB. Data were relative to WT EBL cells without *M. bovis* infection.
1270 (E) Cell adhesion ratio was evaluated via cell adhesion assay after WT EBL cells were infected with
1271 *M. bovis* using High-content imaging. Data were relative to WT EBL cells without *M. bovis*
1272 infection. Scale bar: 20 μm.
1273 (F, G) The expression of epithelial tight junction-related (F) mRNAs (*TJP1*, *CLDN-5*, and *OCLN*)
1274 and (G) proteins (ZO-1, CLDN-5, and OCLN) in *RBMX2* knockout EBL cells after *M. bovis*-infection
1275 through RT-qPCR and WB. Data were relative to WT EBL cells with *M. bovis* infection.
1276 (H) Cell adhesion assay was conducted to assess the cell adhesion ratio of *RBMX2* knockout EBL
1277 cells after infection with *M. bovis*. Data were relative to WT EBL cells with *M. bovis* infection.
1278 Scale bar: 20 μm.
1279 (I) Expression of inflammatory factors-related factors (*IL-6*, *IL-1β*, and *TNF*) were assessed after
1280 *RBMX2* knockout EBL cells infected by *M. bovis*. Data were relative to WT EBL cells with *M. bovis*
1281 infection.
1282 T-test and Two-way ANOVA were used to determine the statistical significance of differences
1283 between different groups. Ns presents no significance, * presents $p < 0.05$, **presents $p < 0.01$,
1284 and *** presents $p < 0.001$ indicate statistically significant differences. Data were representative
1285 of at least three independent experiments.
1286
1287
1288
1289
1290
1291
1292
1293
1294
1295
1296
1297
1298

FIG4

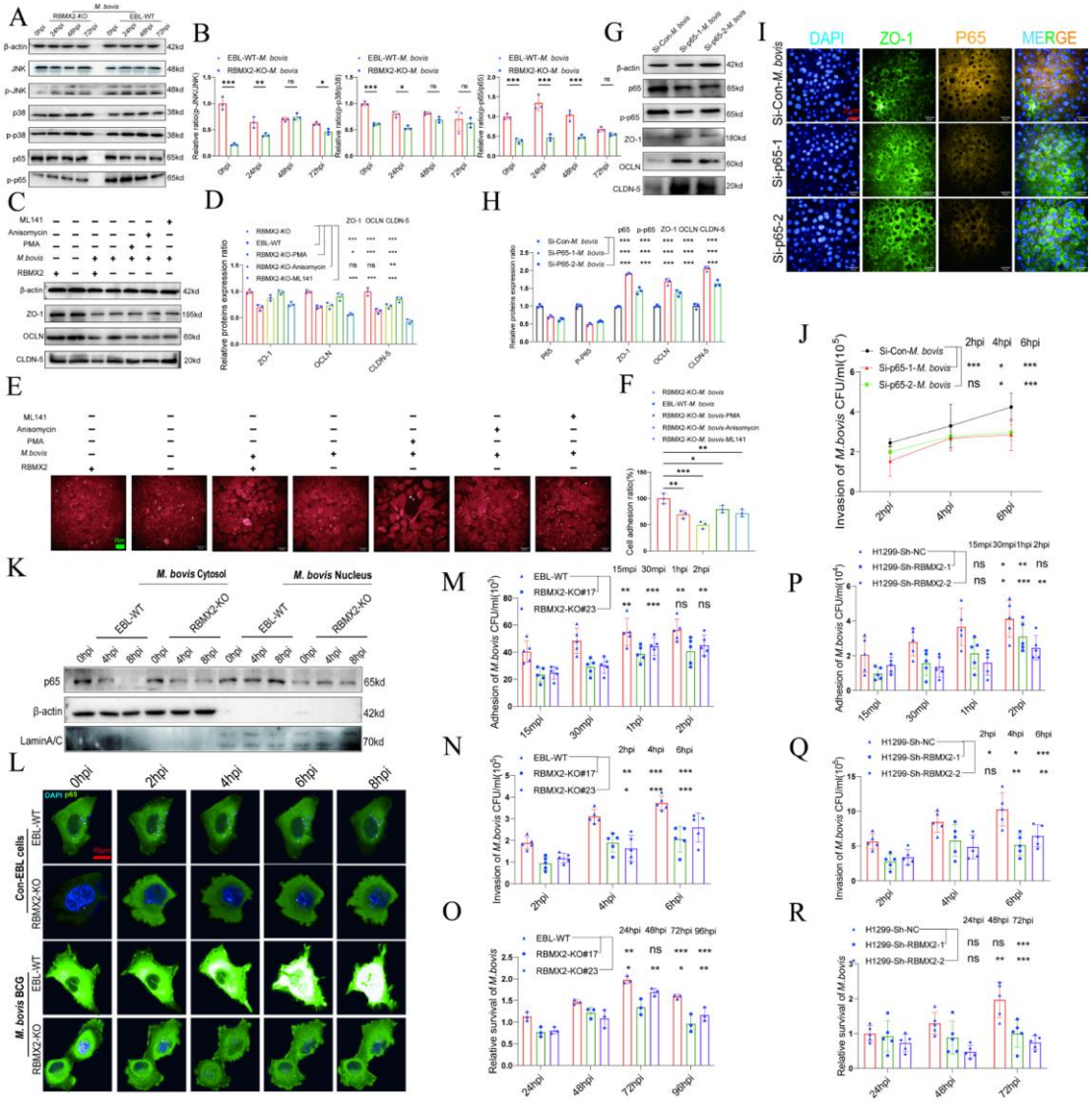
A
B
C
D
E
F
G
H
I
J
K
L
M
N
O
P
Q
R
DAPI
ZO-1
P65
MERGE
Si-Con-M. bovis
Si-p65-1
Si-p65-2
M. bovis Cytosol
M. bovis Nucleus
Invasion of M.bovis CFU/ml(10^5)
Adhesion of M.bovis CFU/ml(10^5)
Relative survival of M.bovis
Cell adhesion ratio(%)

FIGURE 4| *RBMX2* facilitated the disruption of epithelial tight junctions through the promotion of p65 protein phosphorylation and translocation and then enhanced the processes of *M. bovis* adhesion, invasion, and intracellular survival.

(A, B) Activation of the MAPK pathway-related protein and p65 protein were activated after *RBMX2* knockout and WT EBL cells infected by *M. bovis* via WB. Data were relative to WT EBL cells with *M. bovis* infection.

(C, D) Expression of tight junction-related proteins (ZO-1, CLDN-5, and OCLN) was assessed in *RBMX2* knockout EBL cells treated with three p38/p65/JNK pathways activators after *M. bovis* infection via WB. Data were relative to *RBMX2* knockout EBL cells untreated activators with *M. bovis* infection.

(E, F) Evaluate the impact of three *p38/p65/JNK* pathways activators on the ratio of intercellular adhesion via cell adhesion assay. Data were relative to *RBMX2* knockout EBL cells untreated activators with *M. bovis* infection. Scale bar: 20 μm.

(G, H) Evaluate the silencing efficiency of siRNA on p65 protein expression and its impact on the expression of ZO-1, CLDN-5, and OCLN proteins through WB. Data were relative to SiRNA-NC in WT EBL cells with *M. bovis* infection.

(I) Detect the correlation between p65 expression and ZO-1 in WT EBL cells after *M. bovis* infection via IF analysis. ZO-1 is stained with green fluorescence, p65 is stained with yellow fluorescence, and the nucleus is stained with blue fluorescence. Data were relative to SiRNA-NC in WT EBL cells with *M. bovis* infection.

(J) The effect of p65 silencing on the invasive ability of *M. bovis* in WT EBL cells. Data were relative to SiRNA-NC in WT EBL cells with *M. bovis* infection.

(K) The effect of *RBMX2* on the nuclear translocation of p65 protein after *M. bovis* infection using WB. β-actin presents cytosol and Lamin A/C presents nucleus. Data were relative to RBMX2 knockout EBL cells after *M. bovis* infection.

(L) The effect of *RBMX2* on the nuclear translocation of p65 protein after *BCG*-infection using High-content real-time imaging. Using pCMV-EGFP-p65 plasmid transfect RBMX2 knockout and WT EBL cells. The nucleus is stained with blue fluorescence. Data were relative to WT EBL cells without BCG infection.

(M, N, O) The impact of *M. bovis* on the adhesion, invasion, and intracellular survival of *RBMX2* knockout and WT EBL cells through plate counting. Data were relative to WT EBL cells after *M. bovis* infection.

(P, Q, R) The impact of *M. bovis* on the adhesion, invasion, and intracellular survival of Sh-NC and Sh-RBMX2 H1299 cells through plate counting. Data were relative to H1299 ShNC cells after *M. bovis* infection.

One-way ANOVA and two-way ANOVA were used to determine the statistical significance of differences between different groups. Ns presents no significance, * presents $p < 0.05$, **presents $p < 0.01$, and *** presents $p < 0.001$ indicate statistically significant differences. Data were representative of at least three independent experiments.

FIG5

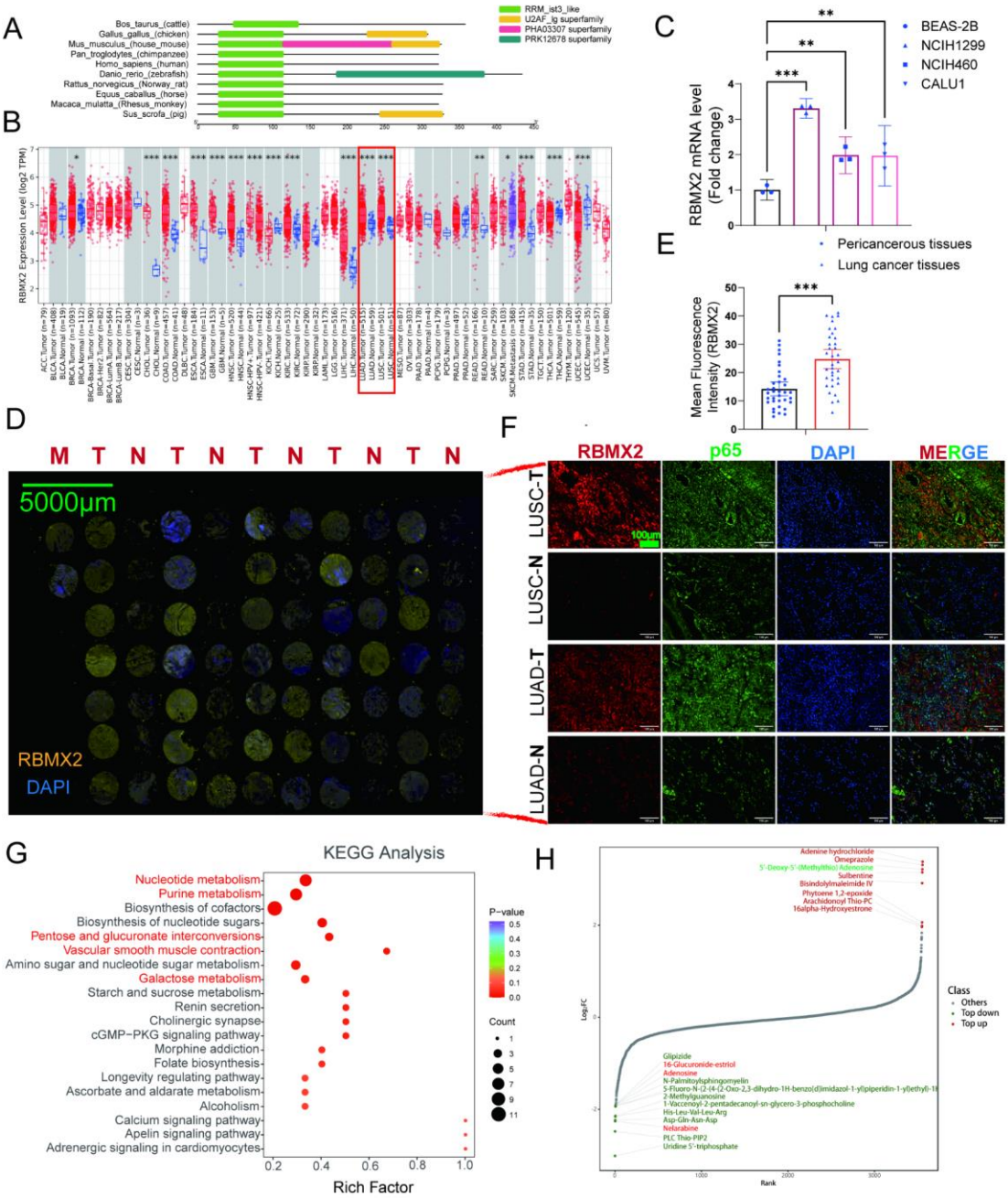
A
RRM_ist3_like
U2AF_lg superfamily
PHA03307 superfamily
PRK12678 superfamily
Bos_taurus_(cattle)
Gallus_gallus_(chicken)
Mus_musculus_(house_mouse)
Pan_troglodytes_(chimpanzee)
Homo_sapiens_(human)
Danio_rerio_(zebrafish)
Rattus_norvegicus_(Norway_rat)
Equus_caballus_(horse)
Macaca_mulatta_(Rhesus_monkey)
Sus_scrofa_(pig)
B
RBMX2 Expression Level (log2 TPM)
C
BEAS-2B
NCIH1299
NCIH460
CALU1
RBMX2 mRNA level (Fold change)
E
Pericancerous tissues
Lung cancer tissues
Mean Fluorescence Intensity (RBMX2)
D
M T N T N T N T N T N
5000μm
RBMX2
DAPI
F
RBMX2
p65
DAPI
MERGE
LUSC-T
LUSC-N
LUAD-T
LUAD-N
100μm
G
KEGG Analysis
Nucleotide metabolism
Purine metabolism
Biosynthesis of cofactors
Biosynthesis of nucleotide sugars
Pentose and glucuronate interconversions
Vascular smooth muscle contraction
Amino sugar and nucleotide sugar metabolism
Galactose metabolism
Starch and sucrose metabolism
Renin secretion
Cholinergic synapse
cGMP−PKG signaling pathway
Morphine addiction
Folate biosynthesis
Longevity regulating pathway
Ascorbate and aldarate metabolism
Alcoholism
Calcium signaling pathway
Apelin signaling pathway
Adrenergic signaling in cardiomyocytes
Rich Factor
P−value
Count
H
Adenine hydrochloride
Omeprazole
5'-Deoxy-5'-(Methylthio) Adenosine
Sulbentine
Bisindolylmaleimide IV
Phytoene 1,2-epoxide
Arachidonoyl Thio-PC
16alpha-Hydroxyestrone
Glipizide
16-Glucuronide-estriol
Adenosine
N-Palmitoylsphingomyelin
2-Methylguanosine
1-Vaccenoyl-2-pentadecanoyl-sn-glycero-3-phosphocholine
His-Leu-Val-Leu-Arg
Asp-Gln-Asn-Asp
Nelarabine
PLC Thio-PIP2
Uridine 5'-triphosphate
Log2FC
Rank
Class
Others
Top down
Top up

FIGURE 5| *RBMX2* is highly expressed in tumor tissues and regulates cancer-related metabolites

(A) A comparative analysis of the functional domains of the *RBMX2* protein across ten different species.

(B) Analyzing the expression patterns of *RBMX2* in pan cancer using *TIMER2.0* cancer database.

(C) The expression of *RBMX2* in different lung cancer cells and normal lung epithelialcells via RT-qPCR. Data were relative to normal lung epithelialcells (BEAS-2B).

(D-E) The expression of *RBMX2* in lung cancer clinical tissues via IF. RBMX2 is stained with yellow fluorescence, and the nucleus is stained with blue fluorescence. Data were relative to pericancerous lung tissues. Scale Bar: 5000 µm.

(F) The expression of *RBMX2* and p65 in LUAD and LUSC clinical tissues via IF. *RBMX2* is stained with red fluorescence, p65 is stained with green fluorescence, and the nucleus is stained with blue fluorescence. Data were relative to normal lung tissues. Scale Bar: 100 µm.

(G) KEGG analysis of differential metabolite enrichment pathways in *RBMX2* knockout EBL cells compared to WT EBL cells after *M. bovis* infection.

(H) Dynamic distribution map of top 20 differential metabolites in RBMX2 knockout EBL cells compared to WT EBL cells after *M. bovis* infection.

FIG6

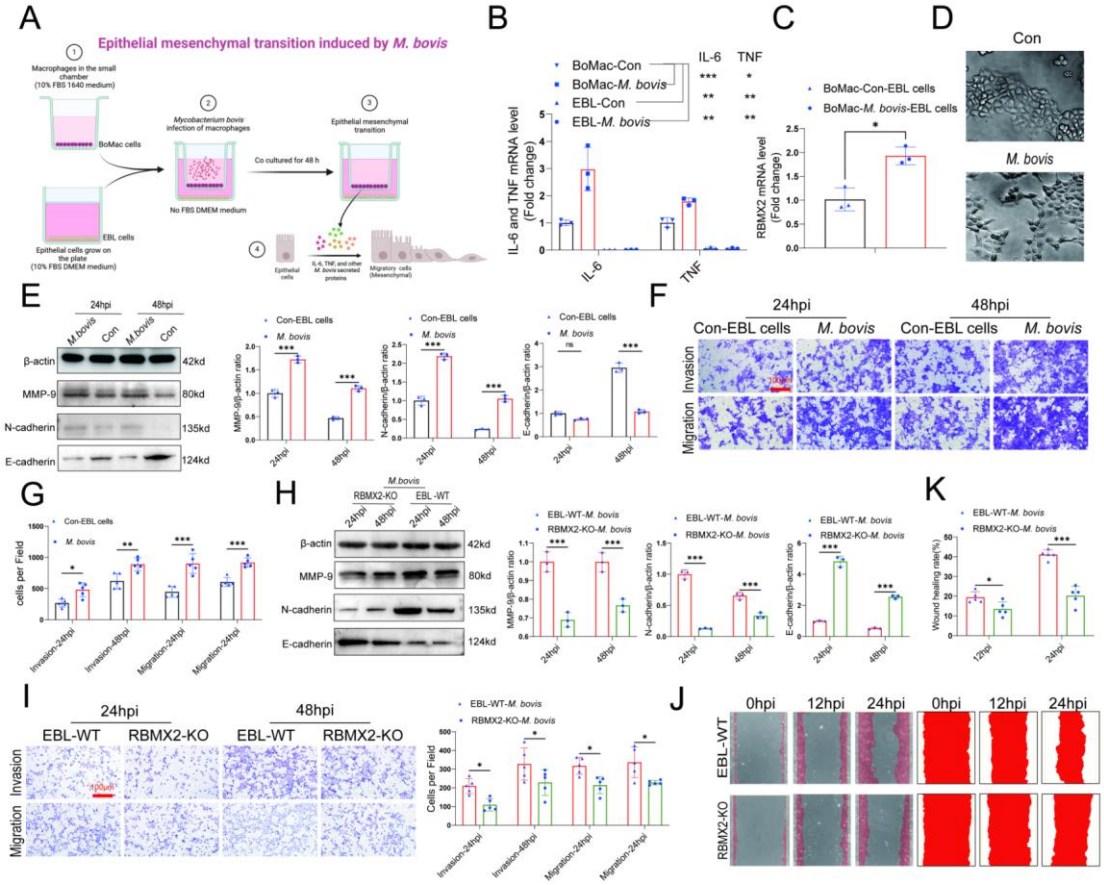
A
Epithelial mesenchymal transition induced by M. bovis
Macrophages in the small chamber (10% FBS 1640 medium)
BoMac cells
EBL cells
Epithelial cells grow on the plate (10% FBS DMEM medium)
Mycobacterium bovis infection of macrophages
No FBS DMEM medium
Co cultured for 48 h
Epithelial mesenchymal transition
Epithelial cells
IL-6, TNF, and other M. bovis secreted proteins
Migratory cells (Mesenchymal)
B
BoMac-Con
BoMac-M. bovis
EBL-Con
EBL-M. bovis
IL-6
TNF
IL-6 and TNF mRNA level (Fold change)
C
BoMac-Con-EBL cells
BoMac-M. bovis-EBL cells
RBMX2 mRNA level (Fold change)
D
Con
M. bovis
E
24hpi
48hpi
M.bovis
Con
β-actin
MMP-9
N-cadherin
E-cadherin
42kd
80kd
135kd
124kd
Con-EBL cells
M. bovis
MMP-9/β-actin ratio
N-cadherin/β-actin ratio
E-cadherin/β-actin ratio
ns
F
24hpi
48hpi
Con-EBL cells
M. bovis
Invasion
Migration
G
Con-EBL cells
M. bovis
cells per Field
Invasion-24hpi
Invasion-48hpi
Migration-24hpi
Migration-24hpi
H
M.bovis
RBMX2-KO
EBL-WT
β-actin
MMP-9
N-cadherin
E-cadherin
42kd
80kd
135kd
124kd
EBL-WT-M. bovis
RBMX2-KO-M. bovis
K
Wound healing rate(%)
12hpi
24hpi
I
24hpi
48hpi
EBL-WT
RBMX2-KO
Invasion
Migration
100μm
Cells per Field
Invasion-24hpi
Invasion-48hpi
Migration-24hpi
Migration-24hpi
J
0hpi
12hpi
24hpi
EBL-WT
RBMX2-KO

1413 **FIGURE 6| *RBMX2* facilitates EMT process in EBL cells after *M. bovis*-infected BoMac cells.**
1414 (A) A pattern diagram illustrated a *M. bovis*-infected BoMac cells inducing EMT of EBL cells
1415 coculture model, drawing by BioRender.
1416 (B) Detection of IL-6 and TNF expression levels in EBL cells and BoMac cells infected with *M. bovis*
1417 using RT-qPCR. Data were relative to BoMac cells without infection of *M. bovis*.
1418 (C) Detection of RBMX2 expression levels in a coculture model EBL cells after *M. bovis* infection
1419 using RT-qPCR. Data were relative to BoMac cells without infection of *M. bovis*.
1420 (D) Observation of morphological changes in EBL cells infected with *M. bovis* under electron
1421 microscopy.
1422 (E) EMT-related proteins (*MMP-9*, *N-cadherin*, and *E-cadherin*) expression was verified in
1423 coculture model EBL cells after *M. bovis* infection through WB. Data were relative to coculture
1424 model EBL cells without *M. bovis* infection.
1425 (F, G) The impact of coculture model EBL cells after *M. bovis* infection on migration and invasion
1426 capacity was detected using Transwell assay. Data were relative to coculture model EBL cells
1427 without *M. bovis* infection.
1428 (H) The detection of EMT-related proteins (*MMP-9*, *N-cadherin*, and *E-cadherin*) of *RBMX2*
1429 knockout EBL cells after *M. bovis-infected* BoMac cells via WB. Data were relative to WT EBL cells
1430 after *M. bovis-infected* BoMac cells.
1431 (I) The change in the migratory and invasive capabilities of *RBMX2* knockout EBL cells after *M.*
1432 *bovis-infected* BoMac cells was assessed via Transwell assay. Data were relative to WT EBL cells
1433 after *M. bovis-infected* BoMac cells.
1434 (J, K) Validate the changes in migration abilities of *RBMX2* knockout EBL cells after *M.*
1435 *bovis-infected* BoMac cells through wound healing assay. Data were relative to WT EBL cells after
1436 *M. bovis-infected* BoMac cells.
1437 T-test and two-way ANOVA were used to determine the statistical significance of differences
1438 between different groups. Ns presents no significance, * presents $p < 0.05$, **presents $p < 0.01$,
1439 and *** presents $p < 0.001$ indicate statistically significant differences. Data were representative
1440 of at least three independent experiments.
1441
1442
1443
1444
1445
1446
1447
1448
1449
1450
1451

1452 FIG7

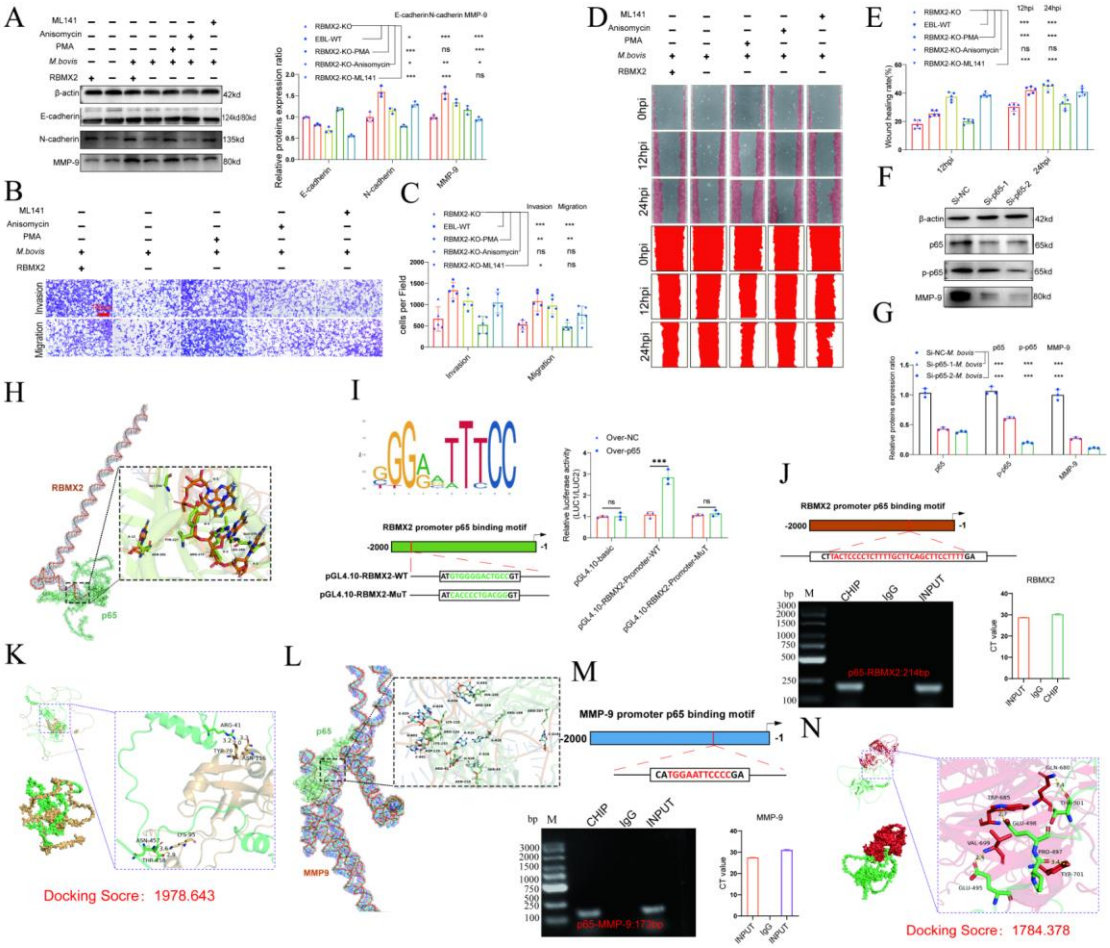

1453

1454

1455

1456

1457

1458

1459

1460

1461

1462

1463

1464

1465

1466

1467 **FIGURE 7| *RBMX2* facilitates the EMT in EBL cells via *p65/MMP-9* pathway.**
1468 (A) Evaluate the impact of pathway activations on expression of EMT-associated proteins (*MMP-9*,
1469 *N-cadherin*, and *E-cadherin*) in *RBMX2* knockout EBL cells after *M. bovis-infected* BoMac cells.
1470 Data were relative to *RBMX2* knockout EBL cells untreated activators.
1471 (B, C) Evaluate the impact of pathway activations on the migratory and invasive capabilities of
1472 RBMX2 knockout EBL cells after *M. bovis-infected* BoMac cells via Transwell assay. Data were
1473 relative to *RBMX2* knockout EBL cells untreated activators.
1474 (D, E) Evaluate the impact of pathway activations on the migratory capabilities of *RBMX2*
1475 knockout EBL cells after *M. bovis-infected* BoMac cells via wound healing assay. Data were
1476 relative to *RBMX2* knockout EBL cells untreated activators.
1477 (F, G) The impact of p65 silencing on the expression of *MMP-9* protein in WT EBL cells after *M.*
1478 *bovis* infection was assessed using WB. Data were relative to SiRNA-NC in WT EBL cells with *M.*
1479 *bovis* infection.
1480 (H) Predicting the binding ability of RBMX2 promoter and p65 using molecular docking dynamics
1481 (I) Verification of *RBMX2* promoter region and p65 interaction using dual luciferase reporter
1482 system.
1483 (I) Using p65 antibody to precipitate p65 protein in EBL cells, and verification of *RBMX2* promoter
1484 region and p65 interaction using Chip-PCR assay.
1485 (K) Predicting potential binding sites for p65 and *RBMX2* via protein docking.
1486 (L) Verification of MMP-9 promoter region and p65 interaction using dual luciferase reporter
1487 system.
1488 (M) Verification of MMP-9 promoter region and p65 interaction using Chip-PCR.
1489 (N) Predicting potential binding sites for p65 and *MMP-9* via protein docking.
1490 Two-way ANOVA was used to determine the statistical significance of differences between
1491 different groups. *$p < 0.05$, **$p < 0.01$, and ***$p < 0.001$ indicate statistically significant
1492 differences. Data were representative of at least three independent experiments.
1493
1494
1495
1496
1497
1498
1499
1500
1501
1502
1503
1504

S1

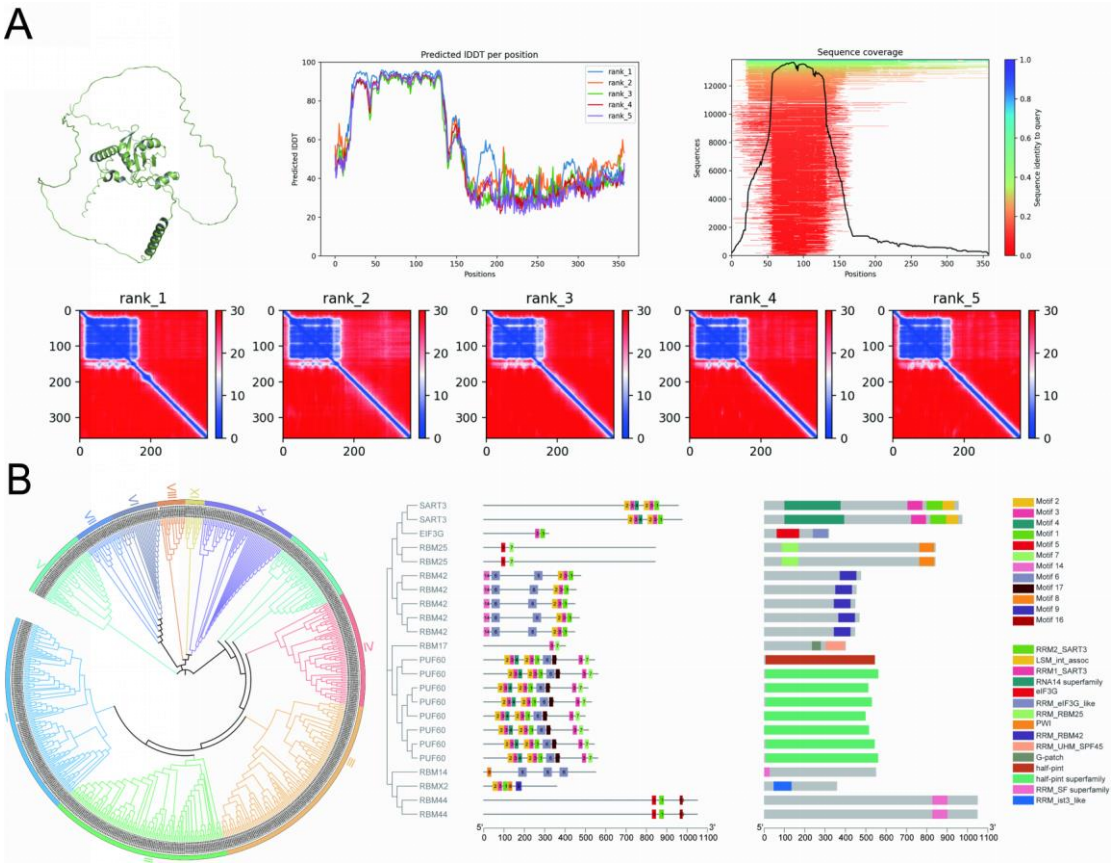

Supplementary Fig 1| Protein structure analysis, subfamily localization.

(A) AlphaFold Multimer predicted the sequence and structure of *RBMX2* protein.

(B) Construction of RBM Gene Family Tree and structural Analysis of genes in *RBMX2* subfamily.

S2

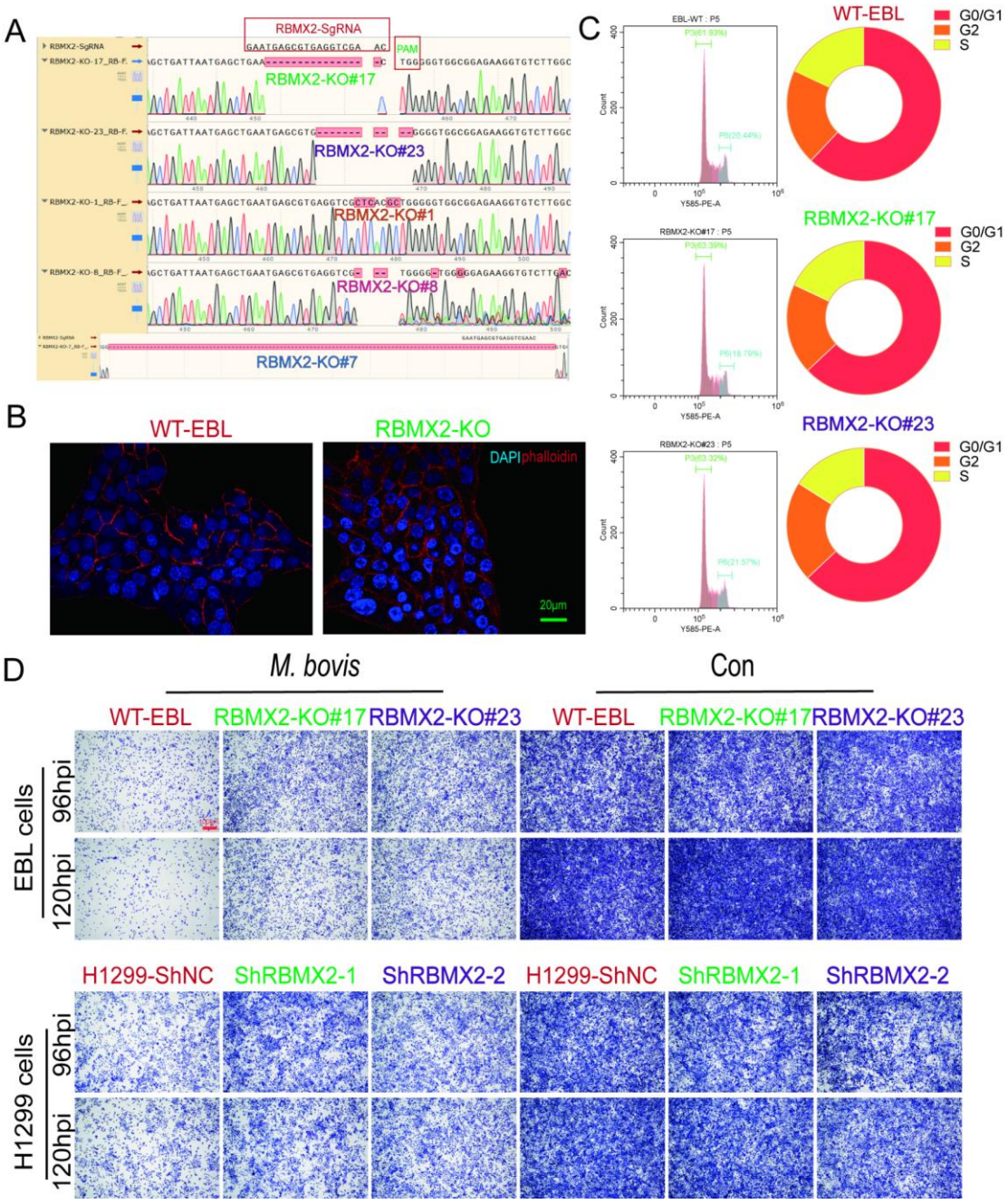
A
RBMX2-SgRNA
PAM
RBMX2-KO#17
RBMX2-KO#23
RBMX2-KO#1
RBMX2-KO#8
RBMX2-KO#7
B
WT-EBL
RBMX2-KO
DAPIphalloidin
20μm
C
WT-EBL
RBMX2-KO#17
RBMX2-KO#23
G0/G1
G2
S
D
M. bovis
Con
WT-EBL
RBMX2-KO#17
RBMX2-KO#23
EBL cells
96hpi
120hpi
H1299-ShNC
ShRBMX2-1
ShRBMX2-2
H1299 cells

Supplementary Fig 2| The influence of *RBMX2* in cell cycle, cell morphology, cell proliferation, and resistance to *M. bovis* infection.

(A) The different knockout sites of *RBMX2* EBL cells were observed by sequencing compared to the bovine *RBMX2* sequence or WT EBL cells.

(B) Using phalloidine to stain the EBL cell skeleton, observing cell morphology under a high-intensity microscope. The cytoskeleton is labeled with red fluorescence, and the nucleus is stained with blue fluorescence. Scale Bar: 20 μm.

(C) Observation of the effect of *RBMX2* knockout on cell cycle of EBL cells by flow cytometry assay. Data are represented as the G0/G1 and S phase relative to WT EBL cells.

(D) The change in cell number of *RBMX2* knockout and silence following 96 and 120 hours of *M. bovis* infection was observed via crystal violet assay in EBL cells and H1299 cells, respectively. Data were represented as the cell number relative to WT EBL cells and H1299-ShNC cells after *M. bovis*-infection. Data were representative of at least three independent experiments.

S3

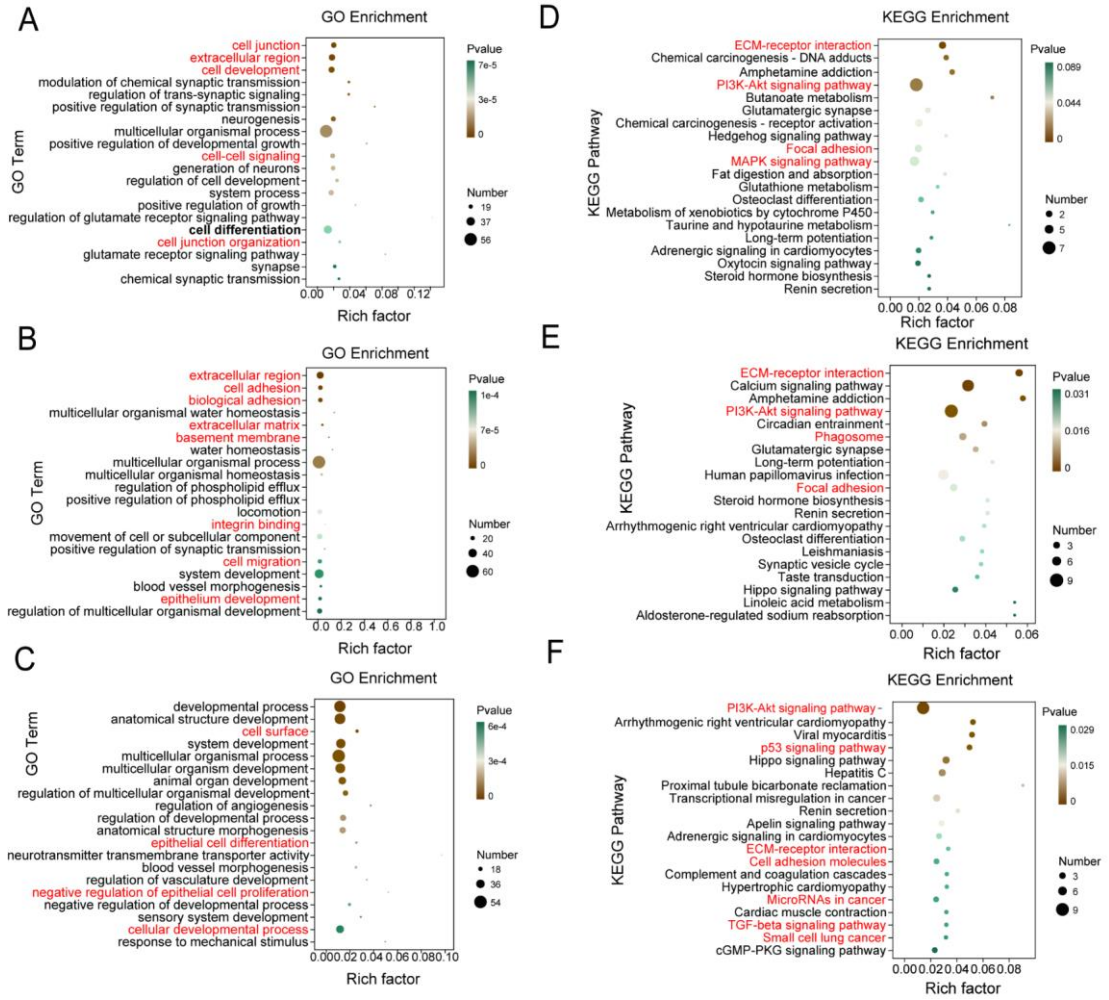

1552

1553 **Supplementary Fig 3| Transcriptome analysis in *RBMX2* knockout and WT EBL cells after *M.***
1554 ***bovis* infection in different time points.**

1555 (A-C) GO analysis of enriched genes of (A) 0 , (B) 24 and (C) 48h after *M. bovis* infection,
1556 respectively. Data were in RBMX2 knockout EBL cells relative to WT EBL cells with *M. bovis*
1557 infection. The changes of these pathways from cell junction-related pathways in 0 hpi to cell
1558 proliferation and differentiation-related pathways in 48 hpi.

1559 (D-F) KEGG analysis of enriched genes of (D) 0, (E) 24 and (F) 48hpi after *M. bovis* infection,
1560 respectively. Data were in RBMX2 knockout EBL cells relative to WT EBL cells with *M. bovis*
1561 infection. The changes of these pathways from inflammation-related pathways in 0 hpi to
1562 cancer-related pathways in 48 hpi.

1563

1564 S4

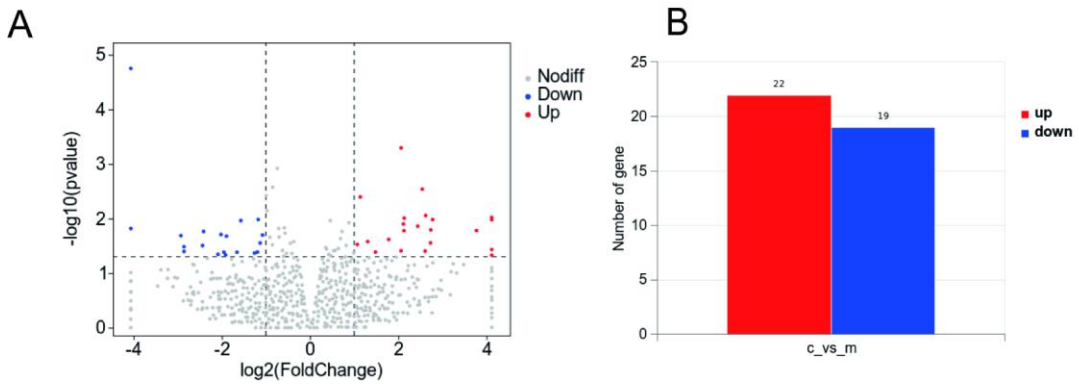

1565

1566 **Supplementary Fig 4| Transcriptomic analysis of *M. bovis* infected EBL cells.**

1567 (A, B) A volcano map illustrating the transcriptional enrichment genes after WT EBL cells with *M.*
1568 *bovis*-infection. Data were relative to WT EBL cells without *M. bovis* infection.

1569

1570

1571

1572

1573

1574

1575

1576

1577

1578

1579

1580

1581 S5

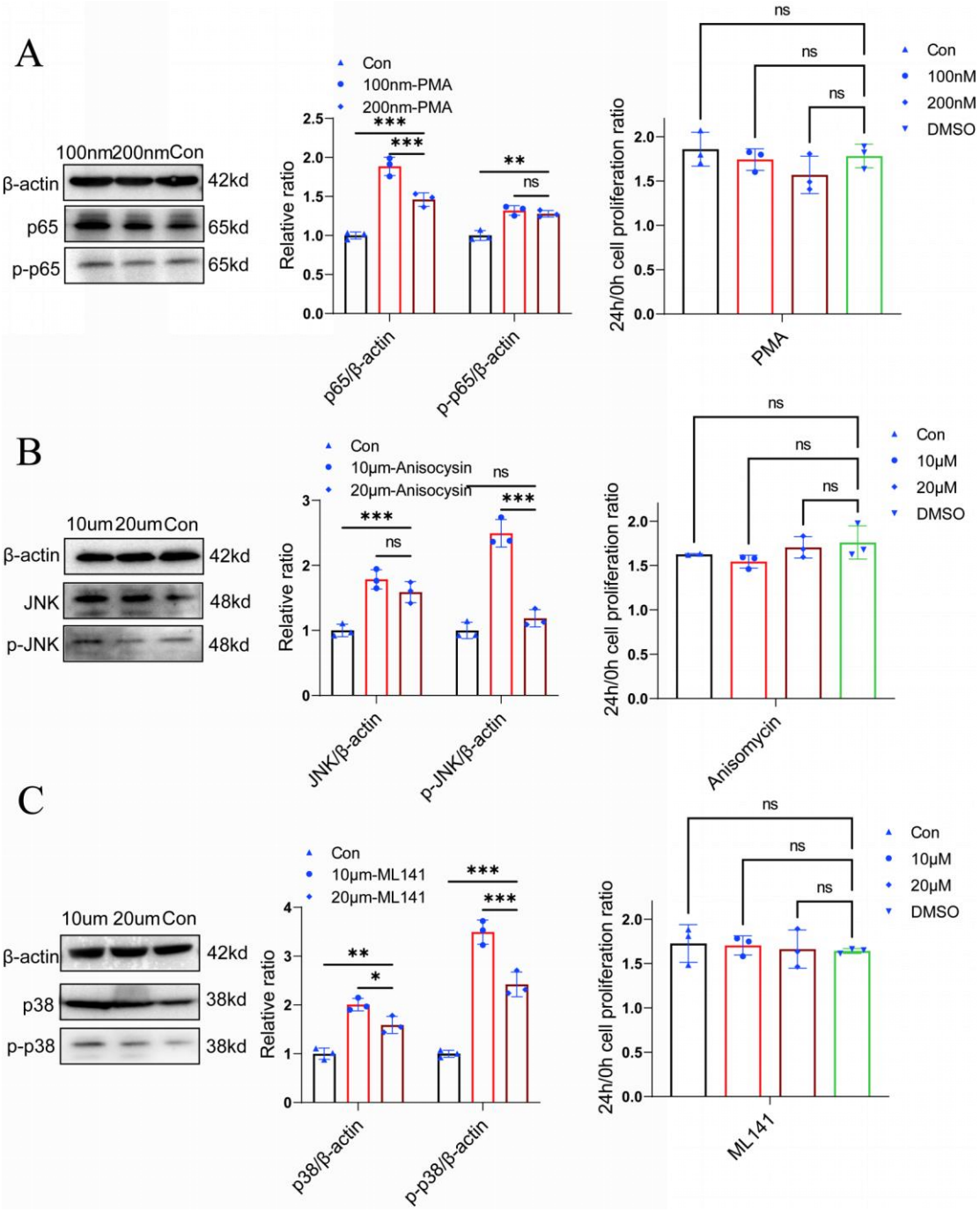

1582

1583 **Supplementary Fig 5| The optimal concentration of activators and their impact on cell viability.**
1584 (A-C) Ascertain the optimal concentration of the three pathway activators and their impact on
1585 cellular viability via WB and CCK-8 assays. Data were relative to WT EBL cells untreated activators.
1586 One-way ANOVA was used to determine the statistical significance of differences between
1587 different groups. Ns presents no significance, **presents $p < 0.01$, and *** presents $p < 0.001$
1588 indicate statistically significant differences.

1589

S6

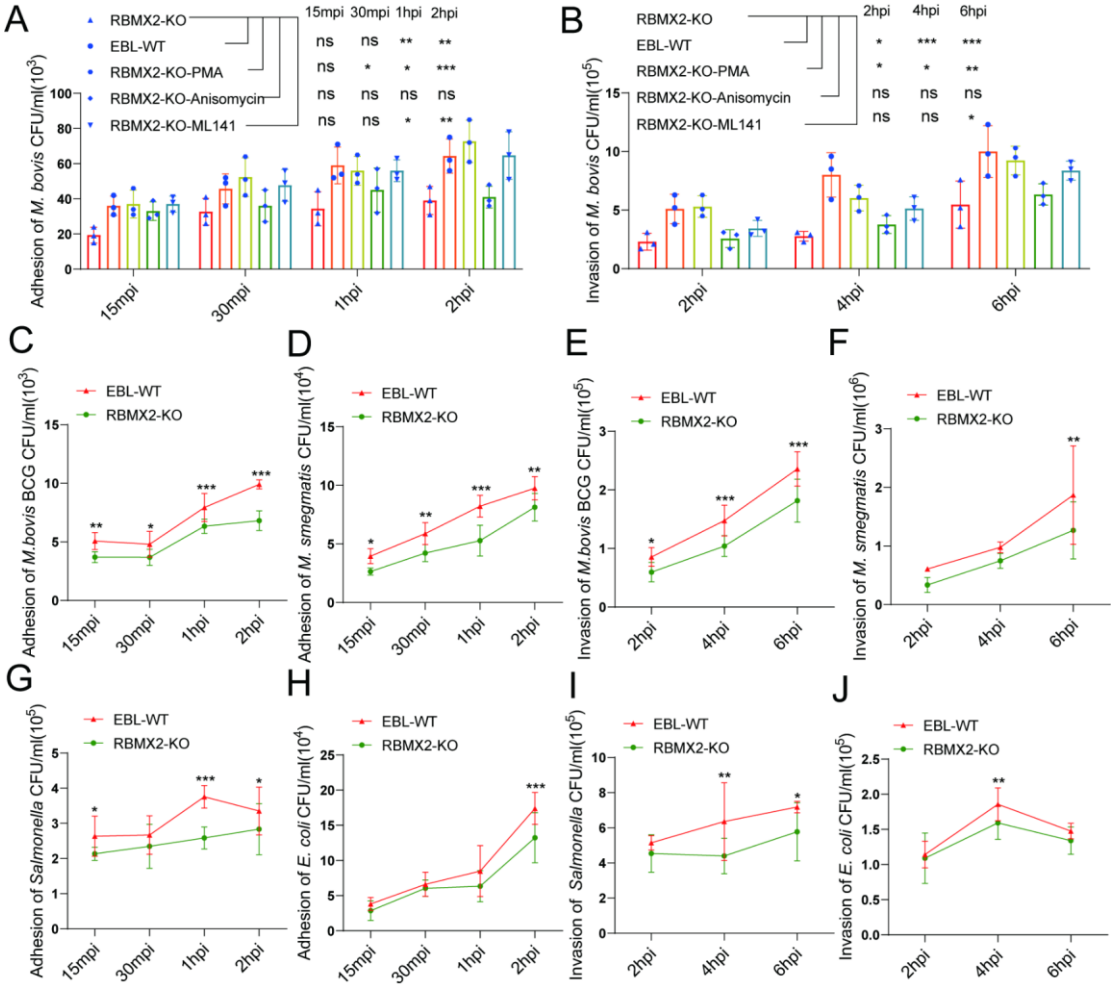
A
RBMX2-KO
EBL-WT
RBMX2-KO-PMA
RBMX2-KO-Anisomycin
RBMX2-KO-ML141
15mpi 30mpi 1hpi 2hpi
Adhesion of M. bovis CFU/ml(10^3)
B
2hpi 4hpi 6hpi
Invasion of M. bovis CFU/ml(10^5)
C
Adhesion of M.bovis BCG CFU/ml(10^3)
D
Adhesion of M. smegmatis CFU/ml(10^4)
E
Invasion of M.bovis BCG CFU/ml(10^5)
F
Invasion of M. smegmatis CFU/ml(10^6)
G
Adhesion of Salmonella CFU/ml(10^5)
H
Adhesion of E. coli CFU/ml(10^4)
I
Invasion of Salmonella CFU/ml(10^5)
J
Invasion of E. coli CFU/ml(10^5)

Supplementary Fig 6| *RBMX2* enhanced the processes of pathogen adhesion, invasion, and intracellular survival.

(A, B) The impact of *M. bovis* on the adhesion and invasion of *RBMX2* knockout EBL cells following treatment with related-pathway activators, verified by plate counting. Data were relative to *RBMX2* knockout EBL cells untreated by activators.

(C, D) The impact of *M. bovis* BCG and *M. smegmatis* on the adhesion of *RBMX2* knockout EBL cells through plate counting assay. Data were relative to WT EBL cells after BCG and *M. Smegmatis* infection.

(E, F) The impact of *M. bovis* BCG and *M. smegmatis* on the invasion of *RBMX2* knockout EBL cells through plate counting assay. Data were relative to WT EBL cells after BCG and *M. Smegmatis* infection.

(G, H) The impact of *Salmonella* and *E. coli*, on the adhesion of *RBMX2* knockout EBL cells through plate counting assay. Data were relative to WT EBL cells after *Salmonella* and *E. coli* infection.

(K, L) The impact of *Salmonella* and *E. coli* on the invasion of *RBMX2* knockout EBL cells through plate counting assay. Data were relative to WT EBL cells after *Salmonella* and *E. coli* infection.

One-way and two-way ANOVA were used to determine the statistical significance of differences between different groups. Ns presents no significance, * presents $p < 0.05$, **presents $p < 0.01$, and *** presents $p < 0.001$ indicate statistically significant differences. Data were representative of at least three independent experiments.

1646

1647 S7

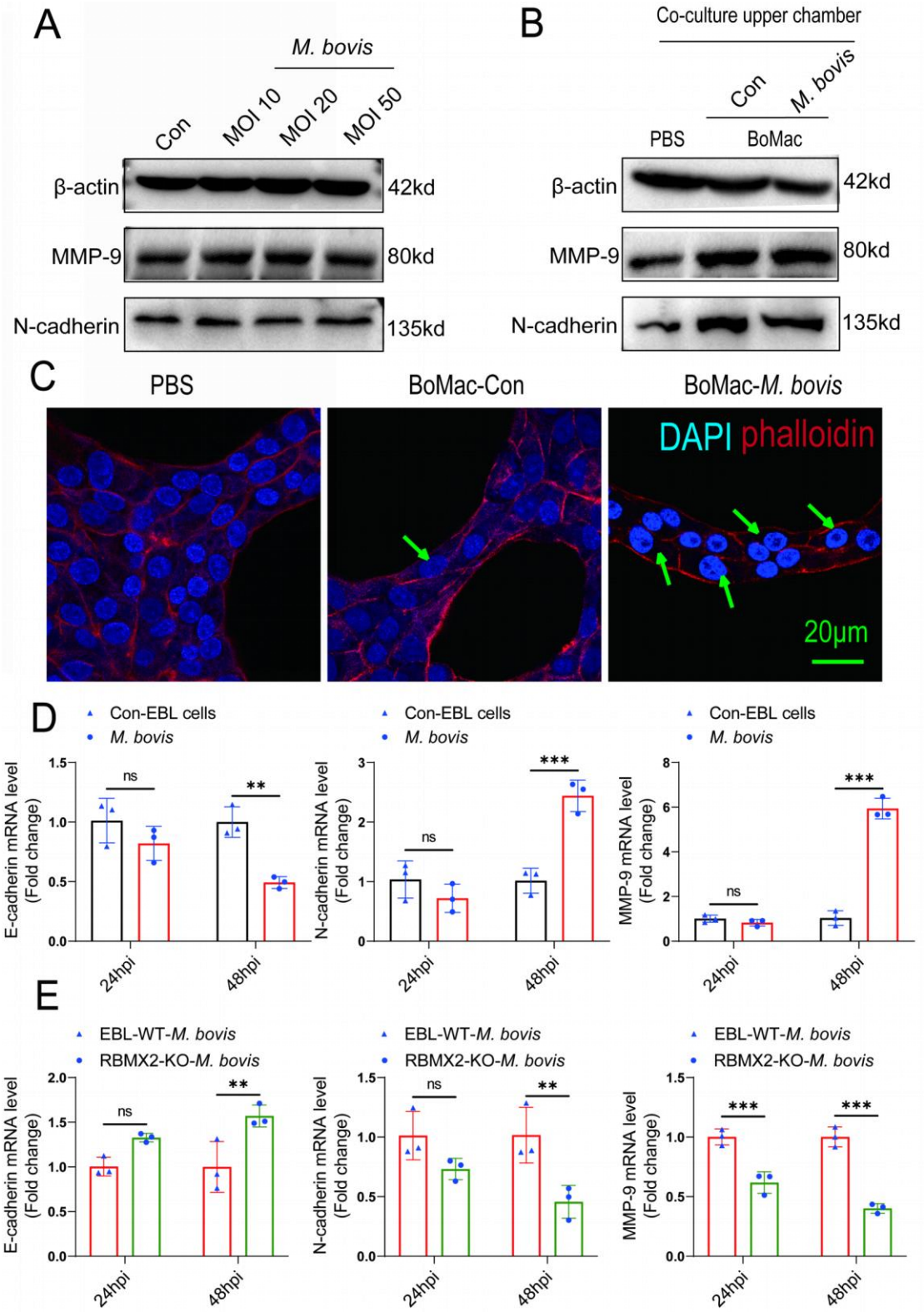

1648

1649

1650

1651

1652 **Supplementary Fig 7| *RBMX2* facilitates EMT process in EBL cells after *M. bovis*-infected BoMac**
1653 **cells.**

1654 (A) WB detection of changes in mesenchymal cell markers (*MMP-9* and *N-cadherin*) after
1655 infection of EBL cells with different infection ratios (10, 20, and 50) of *M. bovis*. Data were relative
1656 to EBL cells without infection of *M. bovis*.

1657 (B) WB detection of the ability of *M. bovis* infection with macrophages (BoMac cells) to induce
1658 epithelial (EBL cells) mesenchymal transition. Data were relative to the addition of PBS in the
1659 upper chamber of the coculture model.

1660 (C) Staining the skeleton of EBL cells in coculture model after *M. bovis* infection using ghost pen
1661 cyclic peptides. The cytoskeleton is labeled with red fluorescence, and the nucleus is stained with
1662 blue fluorescence. Scale Bar: 20 μm.

1663 (D)EMT-related mRNAs (*MMP-9*, *N-cadherin*, and *E-cadherin*) expression was verified in coculture
1664 model EBL cells after *M. bovis* infection through RT-qPCR. Data were relative to coculture model
1665 EBL cells without *M. bovis* infection.

1666 (E) The detection of EMT-related mRNAs (*MMP-9*, *N-cadherin*, and *E-cadherin*) of *RBMX2*
1667 knockout EBL cells after *M. bovis-infected* BoMac cells via RT-qPCR. Data were relative to WT EBL
1668 cells after *M. bovis-infected* BoMac cells.

1669 Two-way ANOVA was used to determine the statistical significance of differences between
1670 different groups. Ns presents no significance, **presents $p < 0.01$, and *** presents $p < 0.001$
1671 indicate statistically significant differences. Data were representative of at least three
1672 independent experiments.

1673

1674

1675

1676

1677

1678

1679

1680

1681

1682

1683

1684

1685

1686

1687

S8

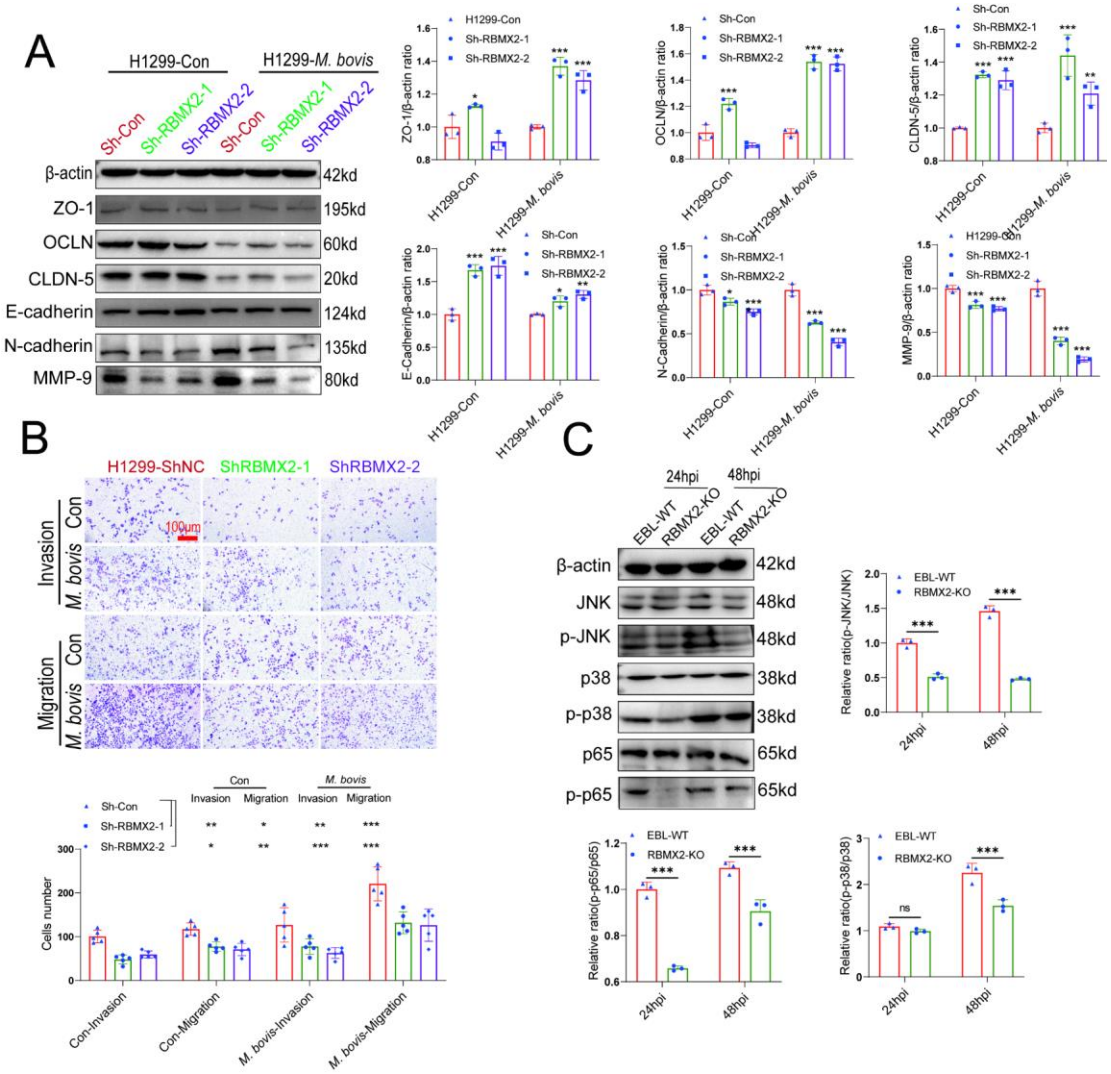

Supplementary Fig 8| *RBMX2* facilitates EMT in H1299 cells.

(A) EMT-related proteins expression was verified in H1299 cells after *M. bovis* infection through WB. Data were relative to H1299 Sh-Con cells.

(B) The change in the migratory and invasive capabilities of H1299 cells was assessed via Transwell assay. Data were relative to H1299 Sh-Con cells. Scale Bar: 100 μm.

(C) Activation of the MAPK pathway-related protein and p65 protein were activated after *RBMX2* knockout and WT EBL cells infected by *M. bovis* in this coculture model via WB. Data were relative to WT EBL cells with *M. bovis* infection.

Two-way ANOVA was used to determine the statistical significance of differences between different groups. $*p < 0.05$, $**p < 0.01$, and $***p < 0.001$ indicate statistically significant differences. Data were representative of at least three independent experiments.

S TABLE 1

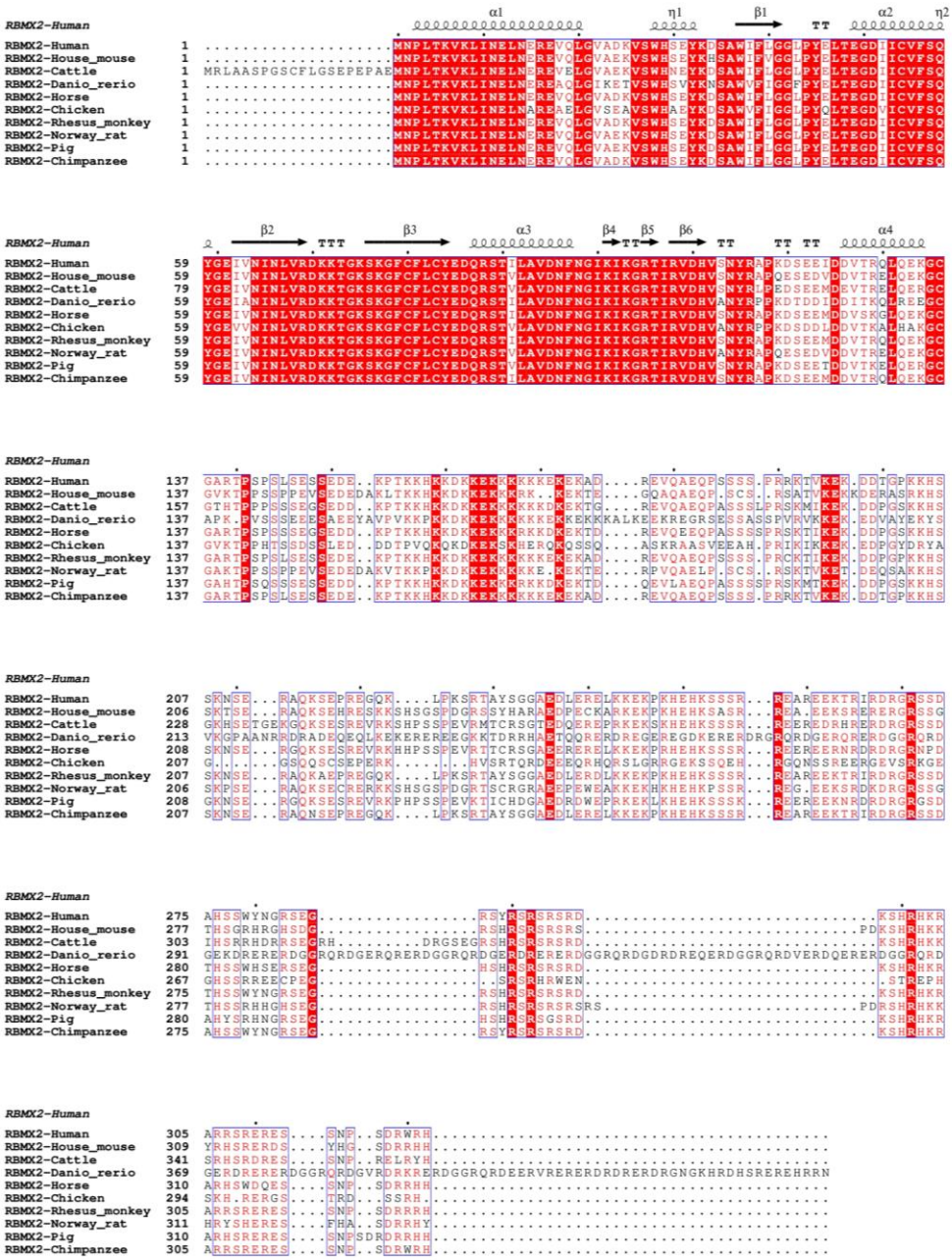

Supplementary Table 1| *RBMX2* exhibits high homology in amino acid sequence alignment across different species